The chemical structure of low-pressure premixed methylcyclohexane flames as benchmarks for the development of a predictive combustion chemistry model

Journal:	*Energy & Fuels*
Manuscript ID:	Draft
Manuscript Type:	Article
Date Submitted by the Author:	n/a
Complete List of Authors:	Skeen, Scott; Sandia Labs, Combustion Research Facility, Combustion Chemistry Yang, Bin; Princeton University Jasper, Ahren; Sandia National Laboratories, Combustion Research Facility Pitz, William; Lawrence Livermore National Laboratory, Chemistry, Material, and Life Sciences Directorate Hansen, Nils; Sandia National Laboratories, Combustion Research Facility

SCHOLARONE™
Manuscripts

The Chemical Structure of Low-Pressure Premixed Methylcyclohexane Flames as Benchmarks for the Development of a Predictive Combustion Chemistry Model

Scott A. Skeen,[*,1] *Bin Yang,*[2] *Ahren W. Jasper,*[1] *William J. Pitz,*[3] *and Nils Hansen*[1]

[1]Combustion Research Facility, Sandia National Laboratories, Livermore, CA 94551, USA

[2]Combustion Energy Frontier Research Center, Princeton University, Princeton, NJ 08540, USA

[3]Lawrence Livermore National Laboratory, Livermore, CA 94550, USA

to be submitted to:

Energy & Fuels

RECEIVED DATE:

[*] Corresponding author: Email: sskeen@sandia.gov; phone: 925-294-2464; fax: 925-294-2276

Abstract

The chemical composition of three low-pressure premixed flames of methylcyclohexane (MCH) is investigated with the emphasis on the chemistry of MCH decomposition and the formation of aromatic species, including benzene and toluene. The flames are stabilized on a flat-flame (McKenna type) burner at equivalence ratios of φ=1.0, 1.75, and 1.9 and at low pressures between 15 Torr (= 20 mbar) and 30 Torr (= 40 mbar). The complex chemistry of MCH consumption is illustrated in the experimental identification of several C_7H_{12}, C_7H_{10}, C_6H_{12}, and C_6H_{10} isomers sampled from the flames as a function of distance from the burner. Three initiation steps for MCH consumption are discussed: Ring opening to heptenes and methyl-hexenes, methyl- loss yielding the cyclohexyl radical, and H abstraction from MCH. Mole fraction profiles as a function of distance from the burner for the C_7 species supplemented by theoretical calculations are presented indicating that flame structures resulting in steeper temperature gradients and/or greater peak temperatures can lead to a relative increase in MCH consumption through the dissociation and isomerization channels. Trends observed among the stable C_6 species as well as 1,3-pentadiene and isoprene also support this conclusion. Relatively large amounts of toluene and benzene are observed in the experiments illustrating the importance of sequential H-abstraction steps from MCH to toluene and from cyclohexyl to benzene. Modeled results using the detailed chemical model of Pitz *et al.* (*Proc. Comb. Inst.* **2007,** 31, 267-275) are also provided to illustrate the use of these data as a benchmark for the improvement or future development of a MCH mechanism.

Keywords: Cycloalkane, flame-sampling molecular-beam mass-spectrometry, methylcyclohexane, premixed flames, low-pressure flames, polycyclic aromatic hydrocarbon

Introduction

A detailed understanding of the combustion chemistry of alkyl-substituted cycloalkanes is well overdue considering their significant presence in practical fuels like gasoline, diesel, and jet fuel.[1] The importance of these cyclic hydrocarbons in practical fuel chemistry will be further enhanced when oil-sand derived fuels emerge, which may contain a larger fraction of cycloalkanes than conventional fuels. An investigation into the combustion chemistry of methylcyclohexane (MCH) is especially interesting in this regard, not just because it is a significant constituent of real fuels, but also because it is widely used to represent the cycloalkane fraction in fuel surrogates for simulating practical combustors.[1-3]

Considering these facts, it is noteworthy that very few MCH combustion chemistry models exist.[2-6] Granata *et al.* reported a semi-detailed model for MCH pyrolysis,[4] which was tested against turbulent flow reactor data from Zeppieri *et al.*[7] An expanded version of this model was later used by Bieleveld *et al.* to model critical conditions of extinction and autoignition of MCH in counter-flow flames.[2] Orme *et al.* presented a detailed kinetic model simulating ignition delay times in shock tubes and earlier flow reactor experiments.[5] Another chemical model was developed by Pitz *et al.* who compared the model's predictions with experimentally measured ignition delay times from a rapid compression machine (RCM).[3] Mittal and Sung compared RCM experiments performed at pressures of 15 and 25 bar and compressed gas temperatures ranging from 680-905 K with modeled results using the mechanism of Pitz *et al.,*[3] and found the predicted ignition delay times to be slightly longer than those measured experimentally.[8] MCH chemistry is also included in JetSurF 2.0,[6] with its performance tested against laminar flame speeds,[9] ignition delay times and OH profiles behind reflected shock waves.[5,10-13]

The predictive capabilities of these combustion chemistry models are best assessed by testing them against reliable, molecule-specific experimental data, for example in the form of species measurements in burner-stabilized flames. However, the lack of such detailed data precludes more extensive testing and possible future improvements of the current MCH combustion chemistry models. In the only available flame chemistry study for MCH combustion, McEnally and Pfefferle reported a limited number of maximum centerline concentrations of various intermediates in coflowing methane/air flames doped with MCH.[14] Although their results were not analyzed with a detailed model, the authors qualitatively concluded that in nonpremixed flames MCH predominantly decomposes by unimolecular dissociation and isomerization, and that a range of aromatics formation pathways are important, which do not include direct dehydrogenation of the ring. This last finding is somewhat surprising considering that in premixed flames pathways exist that form a relatively large abundance of aromatic species via sequential dehydrogenation of cyclic aliphatics containing a six-membered ring.[15-18] For example, benzene formation in fuel-rich cyclohexane flames is dominated by step-wise dehydrogenation, although reactions of small radicals like propargyl, allyl, and *i*-C_4H_5 may also contribute under some conditions.[17,18] In the premixed MCH flames of this work, toluene may be similarly formed via dehydrogenation of the fuel, while benzene may be formed as the dominant aromatic species through fuel decomposition pathways resulting in methyl- loss and an intact six-membered ring followed by dehydrogenation.

Here we describe the detailed chemical structures of three low-pressure (15-30 Torr) premixed MCH flames in the form of species identification and spatially resolved mole fraction data as determined by flame-sampling molecular-beam mass spectrometry. The focus is on experimental evidence for the competition between the several fuel-decomposition routes, i.e.

ACS Paragon Plus Environment

between the dehydrogenation pathway towards toluene, the unimolecular dissociation of the fuel, and the ring-opening reactions followed by decomposition to smaller components. Another aspect of the paper concerns itself with the formation of aromatic species. Altogether, we provide an entirely new set of benchmarks, which is critically needed for future developments of a predictive MCH combustion chemistry model. To better assess the current state of the modeling efforts, the experimental results are compared, wherever deemed appropriate, with predictions of the kinetic model by Pitz *et al.*[3] An updated version of this model is currently under development and will be presented in a future paper.

Experimental Methods

In this study, low-pressure premixed MCH/oxygen/argon flames at equivalence ratios of φ = 1.0, 1.75, and 1.9 are stabilized on a flat-flame McKenna burner at pressures of 15, 20, and 30 Torr, respectively. A summary of the flame conditions is provided in Table 1. Flame A, the stoichiometric flame, provides a more direct investigation of the fuel-consumption/oxidation processes, while the fuel-rich conditions are chosen to produce larger amounts of aromatic species.

Table 1. Flame Parameters

Flame	X_{MCH}	X_{O2}	X_{Ar}	φ	p / Torr	Mass flow rate / g cm^{-2} s^{-1}
A	0.035	0.365	0.60	1.0	15	4.1x10^{-3}
B	0.110	0.640	0.25	1.75	20	4.3x10^{-3}
C	0.060	0.340	0.60	1.9	30	4.3x10^{-3}

The experimental set-up and procedures used to study the chemical composition of such flames have been described in several previous papers.[19-22] The gas flow rates are controlled using calibrated mass flow controllers, and the liquid MCH is metered using a syringe pump, vaporized, and quantitatively added into the oxidizer/Ar stream. Gases from within these flames are extracted using a quartz probe with an orifice diameter of approx. 0.8 mm. The gas-phase species are ionized by single photons with energies between 8-17 eV using tunable synchrotron radiation at the Chemical Dynamics Beamline of the Advanced Light Source located at Lawrence Berkeley National Laboratory. The resulting ions are subsequently separated and detected using a time-of-flight mass spectrometer with a detection limit of ~1ppm.[19]

In a first experiment, the integrated and photon-current normalized ion signals are measured as a function of the photon energy (referred to as an energy scan), thus allowing for identification of the isomeric composition of the combustion intermediates by these so-called photoionization efficiency (PIE) curves. When interpreting the flame-sampled PIE curves, especially for the C_7 intermediates, it is important to realize that many different isomers can contribute to the ion signal at a respective *m/z* ratio.[21] Similar structural features of the isomers can even result in almost identical ionization energies and indistinguishable PIE curves, sometimes precluding an isomer-specific separation of the ion signal. Furthermore, ionization energies and PIE curves for some isomers might not be known and need to be either calculated or measured. A lack of calibration standards (in the form of PIE curves) might make it infeasible to unambiguously identify contributions from isomers with ionization energies above the observed thresholds. Consequently, the species assignments described in this paper do not rely on the observed PIE curves and ionization thresholds alone, but also draw from the current chemical understanding of what intermediates to expect.

In a second experiment, the burner is moved toward or away from the sampling cone to measure the gas composition at different positions within the flame, and the ion signal is then converted into chemical species spatial mole fraction profiles (referred to as a burner scan). The photoionization cross sections, including fragmentation patterns, needed for a quantitative analysis are taken from Refs. [19,23-25]. For some intermediates, the cross sections are estimated by the empirical method of Koizumi or from those of similar molecules.[26] These estimates are summarized in Table 2. To allow for a quantitative determination of the chemical structures of the three model flames, burner scans are performed at energies ranging from 8.8 to 16.6 eV. Burner scans at 8.8, 9.0, 9.5, and 9.8 eV are specifically targeted for the evaluation of the C_7 and C_6 species of interest.

Table 2: Estimated Photoionization Cross-Sections for MCH Combustion Intermediates

Mass	Species	Energy / eV	σ / Mb
98	2-Methyl-1-Hexene	9.5	9.1
98	1-Heptene	9.5	2.5
96	C_7H_{12} (1,3-dienes)	8.8, 9.5, 9.8	8.8, 19.0, 21.0
96	Methyl-Cyclohexenes	9.5, 9.8	9.3, 11.3
94	Lumped C_7H_{10} isomers	8.8	20.0

Mole fraction profiles as a function of distance from the burner are obtained for all three flames for more than 40 species (including radicals) with ion masses ranging from 1 (H) to 98 (C_7H_{14}). Whenever feasible the isomeric contributions at a given ion mass are resolved. For example contributions from allene, vinyl alcohol, and fulvene are separated from propyne, acetaldehyde, and benzene, respectively. However, because of the above discussed issues with

unambiguous isomeric identification, for some of the heavier ion masses, the mole fraction profiles can only be considered partially resolved. Nevertheless, the extensive dataset is uniquely qualified to serve as a test case for future MCH combustion chemistry model improvements or developments. The accuracies of the experimentally determined mole fraction profiles (within 20% for the major species, but as large as a factor of two for intermediates with unknown photoionization cross section) should be sufficient for assessing the predictive capabilities of any new or improved MCH combustion chemistry model. It is not the purpose of this paper to present all available mole fraction profiles, instead only a few critical aspects concerning the fuel consumption and aromatics formation are discussed to guide the model development. The complete dataset is available from the corresponding author upon request.

Flame temperatures, which are important input parameters in modeling calculations, are measured using OH laser-induced fluorescence. A detailed description of the setup is available in the literature.[27] Briefly, light near 306 nm is generated at 10 Hz by an optical parametric oscillator (Continuum, Sunlite EX, FX-1) to excite the OH *A*-*X* (0,0) transition. Measurements are taken approx. 3 cm upstream from the sampling cone tip, thus the temperatures should represent unperturbed conditions. Uncertainties in temperature are estimated to be ± 150 K in the reaction region and post-flame and larger in the preheat zone where the OH concentration diminishes and gradients steepen.

Computational Methods

For some of the potentially important intermediates in the MCH flames, the ionization energies are unknown. To aid in the identification of these species, quantum chemical calculations are performed to calculate the adiabatic and vertical ionization energies. The details

of the present theoretical approach have been described in Refs. [28-31] and are not repeated here. The accuracy of these QCISD(T)/CBS//B3LYP/6-311++G(d,p) calculations has been shown to be excellent, with expected uncertainties of less than 0.1 eV.[28,29]

The unimolecular ring opening and dissociation reactions of MCH are characterized theoretically using multireference perturbation theory (CASPT2), a minimal active space of two electrons and two orbitals, and the cc-pVDZ basis set. This level of theory was previously used to identify competing ring opening mechanisms for cyclohexane.[32] Although this level of theory is not expected to be quantitative, the present CASPT2/cc-pVDZ calculations provide qualitative insights into the unimolecular dissociation of MCH.

To assess the predictive capabilities of the current model by Pitz *et al.,*[3] species mole fraction profiles as function of distance from the burner are computed with CHEMKIN-PRO.[33] The experimental temperature profiles are used as input, thus eliminating the need to solve the energy equation. Mixture averaged transport parameters are used and thermal diffusion is not included.

Global Chemical Flame Structures

Experimental and modeled species mole fraction profiles for H_2, H_2O, CO, O_2, Ar, CO_2, and MCH are shown in Fig. 1 for burner-to-cone distances extending to 30 mm from the burner surface. Agreement between modeled results and experimental data is obtained within the expected accuracies after shifting the measured temperature profile 0.5 mm away from the burner surface for Flame A, 2.5 mm for Flame B, and 2 mm for Flame C to possibly account for perturbations induced by the presence of the quartz probe.[34] The temperature profiles shown in Fig. 1 include these shifts. It should be noted that for all experimental profiles in this paper,

ACS Paragon Plus Environment

"Distance from burner" refers to the actual seperation between the tip of the sampling cone and the burner surface with no correction made. The largest discrepancies between model and experiment exist for the H_2 and H_2O profiles in Flame C; uncertainties in the experimental mole fraction data and/or the temperature profiles cannot be ruled out as an explanation for this observation.

Overall, the results show that the model by Pitz *et al.*[3] is capable of accurately reproducing the global chemical flame structures. However, these major species profiles are largely governed by well known thermochemical parameters and thus depend heavily on the temperature profile that is employed as input to the model calculations. Of greater interest to the present goal of providing new benchmarks for the development of a methylcyclohexane combustion chemistry model, is a detailed understanding of the MCH decomposition and consumption pathways. Experimental insights concerning these aspects are discussed in the following section.

Methylcyclohexane Decomposition and Consumption

In the premixed flames studied here, likely MCH consumption pathways include H-abstraction (from any site on the six-membered ring or from the methyl group) and unimolecular decomposition and isomerization reactions (yielding cyclohexyl+CH_3 or linear and/or branched C_7H_{14} alkenes through ring-opening/H-transfer processes), as shown in Scheme 1.

Unimolecular Isomerization and Decomposition

Experimental evidence for the unimolecular isomerization of MCH to the heptenes and/or methyl-hexenes is found in the form of ion signal at $m/z = 98$ (C_7H_{14}) taken at photon energies

below the ionization threshold of MCH. The known and/or calculated ionization energies of the conceivable C_7H_{14} isomers are summarized in Table 3. The observed threshold near 9.0 eV in the flame-sampled PIE curve in Flame A (Fig. 2a) rules out significant contributions from 2-heptene but suggests the presence of 2-methyl-1-hexene. The distinct change in slope near 9.3 eV is evidence for the presence of 1-heptene and/or the other methyl-hexene isomers. Based on the flame-sampled PIE curve, both 2-heptene and 2-methyl-1-hexene seem to not contribute significantly to the ion signal in Flame C as the threshold appears near 9.3 eV.

Table 3: Ionization Energies of MCH and other Conceivable C_7H_{14} Isomers[a]

Species	Ionization Energy / eV	Reference
Methylcyclohexane	9.64 ± 0.10	35
1-Heptene	9.34 ± 0.08	35
2-Heptene	8.84 ± 0.02	35
2-Methyl-1-Hexene	9.039 ± 0.005	35
3-Methyl-1-Hexene	9.34 (9.73)	calculated, this work
4-Methyl-1-Hexene	9.34 (9.76)	calculated, this work
5-Methyl-1-Hexene	9.32 (9.76)	calculated, this work

[a]Calculated adiabatic ionization energies are tabulated; vertical ionization energies are shown in parentheses.

To experimentally separate these isomerization products from each other is deemed not feasible because all heptenes and methyl-hexenes that are likely to contribute exhibit similar ionization energies (see Table 3) and unknown photoionization cross sections. Nevertheless, partially resolved results are obtained. Experimental mole fraction profiles for the sum of all branched and linear C_7H_{14} species are provided in Fig. 2b for Flames A and C (data for Flame B at the appropriate energy are not available). The profile shape rules out the possibility of the

signal being from impurities of the fuel. We note a quantitative difference between Flames A and C, suggesting that the importance of the isomerization of the fuel is quite sensitive to flame stoichiometry and/or temperature. Also included in Fig. 2b are the sums of the modeled mole fraction profiles for 1-heptene, 2-heptene, and the four methyl-hexenes using the model of Pitz *et al.*[3] The model is capable of accurately reproducing the profile shapes but appears to underpredict the maximum mole fractions. Nevertheless, calibration issues cannot be ruled out as an explanation for the observed discrepancies. In the model calculations, the formation of these isomers occurs via the diradical C_7H_{14} species only, with no direct isomerization reaction being included. But new insights into these rather unusual fuel consumption processes are provided by the following theoretical considerations.

The isomerization reactions (ring-opening/H-transfer) cannot only occur step-wise via one of three diradicals, but also through concerted processes avoiding formation of the diradical intermediates. Competing stepwise and concerted processes have recently been identified for the similar ring opening reactions of cyclohexane[32] and dioxane.[36] A CASPT2/cc-pVDZ potential energy diagram for dissociation via the three diradical intermediates is shown in Fig 3. The threshold for opening to the diradical is 86.4 kcal/mol, which is similar to the threshold for the CH_3 loss channel (84.3 kcal/mol). The diradical can undergo two distinct 1,5-H-atom-transfer reactions, resulting in 2-methyl-1-hexene and 5-methyl-1-hexene with energetic thresholds of 87.7 and 87.1 kcal/mol, respectively. Saddle points associated with concerted processes leading to the methyl-hexenes are also identified with slightly higher thresholds of ~89 kcal/mol. Similar pathways exist for breaking either of the two other C-C bonds in the six-membered ring of MCH, leading to 1- and 2-heptene, and 3- and 4-methyl-hexene (Scheme 1). The calculated threshold energies for all of the unimolecular decomposition processes identified here for MCH are given

ACS Paragon Plus Environment

in Table 4. As expected, the ring opening threshold energies are very similar to those identified previously for cyclohexane.[32] Unfortunately, the concentrations of the diradical C_7H_{14} species (if indeed they are long-lived enough to detect at all) are below the detectable limits of the experimental apparatus.

Table 4. Zero Point Inclusive CASPT2/cc-pVDZ Threshold Energies for the Unimolecular Dissociation and Ring Opening of MCH

Species	Label	ΔH(0 K) / kcal/mol
methylcyclohexane	MCH	0.0
cyclohexyl+CH_3		84.3[a]
1-heptene	1HP	22.5
2-heptene	2HP	20.2
2-methyl-hexene	2MHX	19.4
3-methyl-hexene	3MHX	20.3
4-methyl-hexene	4MHX	20.9
5-methyl-hexene	5MHX	21.1
$CH_2CH_2CH_2CH_2CH_2CH_2CH_2$	D1	83.3
$CH_2CH(CH_3)CH_2CH_2CH_2CH_2$	D2	85.0
$CH_2CH_2CH(CH_3)CH_2CH_2CH_2$	D3	85.0
Concerted ring opening		
[MCH ⇄ 2HP]‡		87.2
[MCH ⇄ 2MHX]‡		88.9
[MCH ⇄ 3MHX]‡		88.4
[MCH ⇄ 4MHX]‡		88.1
[MCH ⇄ 5MHX]‡		88.6
[MCH ⇄ 1HP]‡		87.5
Ring opening to diradicals		
[MCH ⇄ D1]‡		85.5
[MCH ⇄ D2]‡		86.4
[MCH ⇄ D3]‡		85.9
Diradical 1,5 H-transfer		
[D1 ⇄ 1HP]‡		84.2
[D2 ⇄ 5MX]‡		87.1

[D3 ⇄ 4MX]‡	86.7
[D3 ⇄ 3MX]‡	86.8
[D2 ⇄ 2MX]‡	87.7
[D1 ⇄ 2HP]‡	86.3

[a]86.8 kcal/mol at the QCISD(T)/CBS//B3LYP/6-311++G(d,p) level of theory

In addition, low-lying carbene intermediates might compete with the diradical and concerted pathways discussed above.[37] However, the carbene intermediates 1- and 2-heptylidene have CASPT2/cc-pVDZ energies of 102 and 95 kcal/mol, respectively. These energies are more than 10 kcal/mol larger than the diradical intermediates, and we conclude that carbenes are unlikely intermediates for MCH ring opening.

Earlier work suggested that in MCH all of the C-C bonds may dissociate at appreciable rates, but the bonds adjacent to the side-chain break most readily and the C-C bond that connects the methyl group to the ring breaks least readily.[14,38] In contrast, the present ab. initio results indicate that the location of the methyl group has only a minor effect on the threshold energies for ring opening. Our calculations suggest that ring opening is possible via any of the diradicals, and that the four methyl-hexenes and two heptenes are likely to be formed in similar amounts (Scheme 1). Furthermore, the present results suggest that ring opening will compete with the cyclohexyl+CH_3 channel. This methyl loss reaction is energetically the most favored channel, and one might also expect the CH_3 loss channel to be the most favored entropically. However, the number of different ring opening pathways compensates for these energetic and entropic factors, and we estimate that the total rate for ring opening is likely similar to that for CH_3 loss. This conclusion differs from that of a previous study where the CH_3 loss channel was determined

ACS Paragon Plus Environment

to be negligible relative to ring opening.[38] The present calculations are expected to be more reliable than the empirical RRKM estimates of branching given in Ref. [38].

The branched and linear C_7H_{14} isomers are likely to dissociate readily into smaller C_3+C_4 species, because they possess weak allylic C-C bonds.[17,39] Nevertheless, the isomerization and dissociation reactions of MCH are not the only fuel consumption pathways in the premixed flames studied here. While these reactions are likely to be important in the high-temperature region of the flame, H-abstraction reactions forming any of the isomeric C_7H_{13} radicals (Scheme 1) can be assumed to be important close to the burner surface. Possible H-abstraction reactions of the linear and branched C_7H_{14} isomers can lead to heptadienes and methyl-hexadienes. which are also formed from the five different cyclic C_7H_{13} species through ring-opening followed by H-loss. Those reactions are discussed in the following section.

H-Abstraction Reactions and Identification of the C_7H_{12} Intermediates

The different C_7H_{13} radical isomers cannot be distinguished experimentally because the signal intensity is close to the detection limit of the experimental set-up, indicating that these radicals are consumed very fast. Therefore, the focus shifts now to the fate of the initially formed C_7H_{13} radicals, and more information about the MCH consumption under these premixed conditions is obtained by considering the ion signal at m/z = 96 (C_7H_{12}).

Possible H-abstraction and ring-opening reactions (followed by H-abstraction) of the cyclic C_7H_{13} radicals are shown in Scheme 2. According to the study by Orme *et al.,*[5] 1,4- and 1,5-H shifts in the linear and branched C_7H_{13} isomers can be important, thus increasing the number of accessible C_7H_{12} isomers. Following this simple 1- or 2-step scheme, a total of 15

different C_7H_{12} isomers, with ionization energies between 8.19 to 9.52 eV, are possible intermediates. Further details on the different IE's are summarized in Table 4.

We note that the ionization energies of methylenecyclohexane, 3-methyl-cyclohexene and 4-methyl-cyclohexene are too close to be separated experimentally given that the energy resolution of the ionizing photons is E/ΔE~400. Furthermore, the IE's of the conjugated 1,3-dienes are substantially smaller than the IE's of the isolated 1,5- or even 1,6-dienes.

Table 4: Ionization Energies of C_7H_{12} Isomers Likely to be Detected in MCH Flames[a]

Species	Ionization Energy / eV	Reference
Methylenecyclohexane	8.93±0.01 (9.13)	35
1-Methyl-Cyclohexene	8.67±0.02 (8.69±0.05)	35
3-Methyl-Cyclohexene	8.89±0.01 (9.12)	35
4-Methyl-Cyclohexene	8.91±0.01	35
1,3-Heptadiene	(E) 8.47	35
1,5-Heptadiene	9.00 (9.31)	calculated, this work
1,6-Heptadiene	(9.52±0.02)	35
2,4-Heptadiene	(8.17)	35
2-Methyl-1,5-Hexadiene	9.09 (9.40)	calculated, this work
3-Methyl-1,5-Hexadiene	9.15 (9.60)	calculated, this work
2-Methyl-1,3-Hexadiene	8.39 (8.63)	calculated, this work
3-Methyl-1,3-Hexadiene	8.34 (8.58)	calculated, this work
4-Methyl-1,3-Hexadiene	(E) (8.19)	35
5-Methyl-1,3-Hexadiene	(trans) (8.47)	35
2-Propyl-1,3-Butadiene	8.78 (8.99)	calculated, this work

[a]Adiabatic ionization energies are tabulated; vertical ionization energies are shown in parentheses.

A flame-sampled photoionization efficiency (PIE) curve for *m/z* = 96 (C_7H_{12}) is shown in Fig. 4, also indicating the ionization energies of several of the intermediates that are possibly present. While the cyclic species methylenecyclohexane, 1-methylcyclohexene, 3-methylcyclohexene, and 4-methylcyclohexene are likely candidates to be present in the flame, their ionization energies are above the observed threshold of ~8.5 eV in the flame-sampled PIE curve. This threshold indicates the presence of linear and/or branched 1,3-dienes. Potential formation pathways for 1,3-heptadiene are indicated in Scheme 2 and begin with ring opening of the cyclohexyl-methylene, the 1-methyl-cyclohex-2-yl, or the 1-methyl-cyclohex-3-yl radical yielding 1-hepten-7-yl, 2-hepten-7-yl, or 1-hepten-6-yl, respectively. The formation of the resonance-stabilized and more stable 1-hepten-3-yl radical and 2-hepten-4-yl radicals leading to 1,3-heptadiene requires a hydrogen transfer via a 5- or 6-membered ring transition state. All other similar ring-opening processes of the other C_7H_{13} radicals followed by H-transfer and -loss are summarized in Scheme 2. Based on the observed ionization threshold of ~8.5 eV in the flame-sampled PIE curve, we conclude that mole fractions of 2,4-heptadiene and 4-methyl-1,3-hexadiene are below the detectable limit of ~1 ppm.

Alkenes with isolated C=C double bonds are characterized by IE's above 9 eV and their presence is difficult to verify because of the large amount of possible isomers with lower IE's. In other words, a lack of PIE curves for 1,3-dienes and the methylcyclohexene isomers prevents an assessment of their individual contributions to the signal at *m/z* = 96. However, it can be expected that more 1,3-dienes would be present in the flame when compared to other diene isomers. The detection of 1,3-diene also implies that the 1,4- and 1,5-H shifts are of comparable rate to the β-scission of the C-C bonds that result in smaller fragments. Due to degeneracy, the rate for H-atom abstraction from the *ortho*- and *meta*-carbon sites dominates over the other H-

abstraction rates. Thus, one might expect more 3- and 4-methylcyclohexene than 1-methylcyclohexene in the flame. And in fact, the flame-sampled PIE curve in Fig. 4 provides supporting evidence where a distinct change in slope is observed near the ionization thresholds of 3- and 4-methylcyclohexene.

Mole fraction profiles as function of distance from the burner for the C_7H_{12} species are obtained at two photon energies as shown in Fig. 5. The experimental mole fraction profiles representing mainly the 1,3-dienes (but also some 1-methylcyclohexene) are obtained at 8.8 eV. Mole fraction profiles representing the sum of all C_7H_{12} isomers are obtained at 9.5 eV (Flames A and C) and at 9.8 eV (Flame B). Comparing the mole fraction profiles of the three flames, the data indicate larger peak mole fractions in the stoichiometric flame with a greater total spatially integrated amount in the fuel-rich flame at $\varphi = 1.9$.

With regards to the model, all of the species in Table 4 are included in the mechanism of Pitz *et al.*[3] with the exception of 2-propyl-1,3-butadiene. Also, a lumped species is used to represent the methylcyclohexene isomers. In Fig. 5, the modeled mole fraction profiles representing the sums of all C_7H_{12} isomers are included, and we observe that the current model seems to underpredict the mole fraction of these species by about one order of magnitude.

By comparing the spatially integrated experimental mole fractions of the linear and branched $m/z = 98$ isomers (C_7H_{14}, Fig. 2b) with the lumped C_7H_{12} species (Fig. 5) we can assess the significance of the initial MCH consumption pathways. To estimate the upper limits for MCH consumption via isomerization reactions and unimolecular dissociation yielding cyclohexyl+CH_3, we assume that the integrated mole fraction profiles scale with the relative rates of MCH consumption and that the C_7H_{12} profile is representative of all of the H-abstraction reactions. Given that the integrated mole fraction of the lumped heptenes and methyl-hexenes is

ACS Paragon Plus Environment

approx. 22% of the peak C_7H_{12} mole fraction for Flame A and assuming, as discussed above, similar rates for unimolecular dissociation and isomerization, we conclude that for Flame A ~70% of MCH is consumed via H-abstraction, 15% via isomerization, and 15% via unimolecular dissociation. For Flame C, a similar analysis indicates that 75% of MCH is consumed via H-abstraction, 13% via isomerization, and 13% via unimolecular dissociation. Although large error bars are associated with these numbers, it seems that a slightly larger percentage of MCH is consumed via H-abstraction in the fuel-rich flame, which can be attributed to the rapid diffusion of H atoms from the reaction region back to the burner surface and the greater flame stand-off distance which results in delayed consumption by the dissociation and isomerization routes. In the stoichiometric flame, the flame resides closer to the burner surface resulting in a much steeper temperature gradient and greater competition between the various reaction pathways.

It is noteworthy that McEnally and Pfefferle concluded for non-premixed flames that unimolecular dissociation, not H-abstraction, dominates cycloalkane decomposition.[14] Although their experimental set-up did not allow isomer-specific measurements, they infer that the primary dissociation reaction for MCH is ring opening isomerization to form 1- and 2-heptene. These results are in qualitative agreement with our study which clearly indicates (through the direct measurement of the linear and/or branched C_7H_{14} isomers) that isomerization of the fuel is an important fuel-consumption pathway.

C_7H_{13} Radical Decomposition Reactions

The decomposition of the initially formed C_7H_{13} radicals can also be seen in the PIE curves of *m/z* = 84 (C_6H_{12}) and *m/z* = 68 (C_5H_8). The PIE curve for *m/z* = 84 (Fig. 6) shows an initial rise in signal near 9.0 eV, indicating the presence of linear and/or branched alkenes with

the empirical formula C_6H_{12}. These species cannot be direct products resulting from fuel decomposition, but may form via methyl radical addition to C_5H_9 radicals. Both radical species are assumed to be present in larger concentrations, because they are readily formed fuel-decomposition products. As shown in Scheme 3, C_5H_9 radicals can be formed from the initial C_7H_{13} radicals via ring-opening and subsequent β-scission. As can be seen, five isomeric C_5H_9 radicals can be formed, and if they should recombine with methyl radicals, the following C_6H_{12} isomers are likely to be detected: 2-hexene (IE = 8.97 eV), 2-methyl-1-pentene (IE = 9.08 eV), 1-hexene (IE = 9.44 eV), 3-methyl-1-pentene (IE = 9.44 eV), and 4-methyl-1-pentene (IE = 9.45 eV). The observed threshold near 9.0 eV matches the ionization energy of 2-hexene, but contributions from methyl-pentene isomers cannot be ruled out. Mole fraction profiles are not presented here, because the C_6H_{12} isomers appear only at relatively low concentrations. All these C_6H_{12} isomers have allylic C-C bonds and it is likely that these species decompose readily into C_2, C_3, and C_4 fragments.

The mechanism of Pitz *et al.*[3] includes 1-, 2-, and 3-hexene along with four methyl-pentene isomers (2-methyl-1-pentene, 2-methyl-3-pentene, 4-methyl-2-pentene, and 4-methyl-1-pentene). But only 4-methyl-2-pentene and 3-hexene are formed via methyl + C_5H_9 radical reactions. Other included reactions involve CH_3 addition to C_5H_{10} species, which yield C_6H_{13} and subsequently C_6H_{12} after H-abstraction.

As mentioned above, β-scission of the branched and linear C_7H_{13} radicals leads to various C_5H_9 radical isomers. Subsequent H-abstraction or -loss can produce 1,3-pentadiene, isoprene (2-methyl-1,3-butadiene), and 1,4-pentadiene. In the flame sampled PIE curve shown in Fig. 7, ion signal from 1,3-pentadiene (IE = 8.6 eV) is observed at the threshold while there is evidence for the presence of isoprene based on the divergence of the flame sampled PIE curve and that of the

ACS Paragon Plus Environment

1,3-pentadiene cold gas near 8.9 eV. Ion signal from cyclopentene cannot be confirmed; however, the change in slope of the flame sampled PIE curve near 9.6 eV may be due to 1,4-pentadiene. Experimental mole fraction profiles for 1,3-pentadiene and isoprene are provided in Fig. 8. The 1,3-pentadiene mole fraction is evaluated at 8.8 eV. In Flames A and C the isoprene mole fraction is evaluated at 9.0 eV, while in Flame B isoprene is evaluated at 9.2 eV. Because possible contributions to the ion signal from cyclopentene are possible at 9.2 eV, the uncertainty in the isoprene mole fraction profile for Flame B is greater.

Under the assumption that the C_5H_8 species are mainly formed through MCH decomposition initiated by H-abstraction, a comparison of the three spatially integrated isoprene mole fraction profiles normalized by the respective fuel-inlet mole fractions can yield information regarding differences in the flame-specific amount of MCH consumption via H-abstraction. The results indicate that H-abstraction is more prevalent in Flame C than in Flame A (as discussed above) and least prevalent in Flame B.

With regard to the modeled results, we observe good agreement (within a factor of two) for isoprene and 1,3-pentadiene in all flames with the exception of the 1,3-pentadiene profile in Flame B, which is overpredicted by a factor of 5. The modeled mole fraction profiles for 1,4-pentadiene and cyclopentene are lower than that of isoprene and 1,3-pentadiene by more than one order of magnitude and are therefore not included in the figure.

Formation of Aromatic Species

Earlier work revealed that the fuel structure has some influence on how aromatic species are formed in flames.[17] From the above discussion of the fuel decomposition and consumption processes it is obvious that in the MCH flames studied here, direct pathways toward aromatic

species exist. In detail, toluene could be formed through several dehydrogenation steps directly from the fuel, while benzene could be formed after methyl-loss and dehydrogenation of the resulting cyclohexyl radical. Experimental evidence for these routes, which is contained in the signal at *m/z* = 94 (C_7H_{10}), 92 (C_7H_8), 82 (C_6H_{10}), 80 (C_6H_8) and 78 (C_6H_6), is presented in the following paragraphs.

Successive Dehydrogenation Towards Toluene

The flame-sampled PIE curve for *m/z* = 94 is shown in Fig. 9 and the IE's of the C_7H_{10} isomers likely to be present in the MCH flames are summarized in Table 5. The cyclic C_7H_{12} species, identified to contribute to the ion signal at *m/z* = 96 (Fig. 4), can further dehydrogenate and form different cyclic C_7H_{10} isomers. Dehydrogenation of the branched heptadiene and methyl-hexadiene structures at *m/z* = 96 will likely lead to heptatrienes and methyl-hexatrienes with IE's of 7.96 eV and ~8.1 eV

Table 5: Ionization Energies of C_7H_{10} Isomers Likely to be Detected in MCH Flames[a]

Species	Ionization Energy / eV	Reference
(E,E)-1,3,5-Heptatriene	7.96 (8.16)	35,40
(E)-2-Methyl-1,3,5-Hexatriene	8.15 (8.33)	calculated, this work
(Z)-2-Methyl-1,3,5-Hexatriene	8.16 (8.34)	calculated, this work
(E)-3-Methyl-1,3,5-Hexatriene	(8.28)	35
1-Methyl-1,3-Cyclohexadiene	7.95 (8.18)	calculated, this work
2-Methyl-1,3-Cyclohexadiene	8.05 (8.29)	calculated, this work
5-Methyl-1,3-Cyclohexadiene	8.21 (8.43)	calculated, this work
1-Methyl-1,4-Cyclohexadiene	8.67 (8.96)	calculated, this work
3-Methyl-1,4-Cyclohexadiene	8.79 (9.06)	calculated, this work

[a]Adiabatic ionization energies are tabulated; vertical ionization energies are shown in parentheses.

In Fig. 9, ion signal is observed at the lowest photon energy used in these experiments indicating the possible presence of 1,3,5-heptatriene, 1-methyl-1,3-cyclohexadiene, and/or 2-methyl-1,3-cyclohexadiene. Although formation pathways to the methyl-hexatriene and heptatriene isomers can be inferred, significant concentrations of these species are not likely to be observed in the flames considering the bond-strength of allylic carbon-carbon bonds, the likely β-scission routes for the straight-chain and branched smaller radical species, and the greater stability of the cyclic isomers.

Experimental mole fraction profiles for the sum of all C_7H_{10} species ionized at 8.8 eV are shown in Fig. 10. Modeled results using the chemical kinetic mechanism of Pitz *et al.*[3] are also included with the profiles of all C_7H_{10} isomers combined into one curve. All species from Table 5 are included in this mechanism; however, the methylcyclohexadiene isomers are lumped. The model predicts mainly 1,3,5-heptatriene and 2-methyl-1,3,5-hexadiene, with the lumped methylcyclohexadiene isomers contributing modestly only in the stoichiometric flame.

Further dehydrogenation of the C_7 species, leads to toluene, which is identified experimentally to be the only isomer at m/z = 92 (C_7H_8). Its experimental and modeled mole fraction profiles for all flames are shown in Fig. 11 and we note that for all three flames the model appears to underpredict the toluene mole fraction, especially for the stoichiometric case (Flame A). In Fig. 11a the experimental toluene mole fraction profile from the stoichiometric cyclohexane (CHX) flame of Law *et al.*[16] is included. Also included in Fig. 11c is the toluene mole fraction profile from a fuel-rich ($\varphi = 2.0$) 1-hexene flame.[39] The profile from the CHX flame provides an indication of the propensity to form toluene via reactions involving the six-

membered ring, while the profile from the 1-hexene flame from Ref. 39 is thought to provide a reasonable indication of the upper limit of toluene that might form from linear fuels. As evidence for the importance of MCH dehydrogenation leading to toluene, it can be seen that the stoichiometric MCH flame produces nearly 20 times more toluene than the stoichiometric CHX flame. Comparing the profile from the 1-hexene flame, it can be seen that the fuel-rich MCH flame produces approx. five times more toluene.

An accurate analysis of the relative contribution of H-abstraction reactions leading to toluene is done through a comparison of the ratios of the spatially integrated amounts of toluene to the C_7H_{10} species. Assuming that the majority of the C_7H_{10} species are cyclic, the conversion of the methyl-1,3-cyclohexadienes to toluene presumably via H-abstraction is more efficient in Flame C than in Flame A and least efficient in Flame B. Given the significantly larger peak temperature of Flame B, this result supports the argument that higher temperatures lead to a relative increase in dissociation and/or isomerization routes.

Benzene Formation Through Fuel Decomposition and Dehydrogenation

As discussed above, according to our analysis, about 15% of the MCH is consumed via unimolecular dissociation forming methyl and cyclohexyl radicals. The fact that the six-membered ring stays intact through the initial step of fuel consumption offers the possibility to subsequently form benzene through dehydrogenation steps. However, cyclohexyl radicals can also be formed from H-abstraction reactions followed by β-scission (Scheme 2). The stepwise dehydrogenation pathway was found to be dominant in stoichiometric and fuel-rich cyclohexane flames and is likely to contribute also in the MCH flames studied here.[15-17] The following evidence for the importance of this reaction sequence is found in the experimental data.

At *m/z* = 82 (C_6H_{10}) the onset at 8.95 eV in the flame-sampled PIE curve of Fig. 12 is due to the ionization of cyclohexene. The observed signal at lower photon energies can be assigned to contributions of linear and or branched dienes likely to be formed via dehydrogenation steps from the respective C_6H_{12} isomers. Conceivable isomers are 2-methyl-1,3-pentadiene (IE = 8.47 eV), 3-methyl-1,3-pentadiene (IE = 8.46 eV), and 1,3-hexadiene (IE = 8.54 eV), with their ionization energies being very close to the observed threshold near 8.5 eV. For the possible 1,3-dienes only the PIE curve for 1,3-hexadiene is shown as the others are not presently available. Significant contributions from 2,4-hexadiene and 4-methyl-1,3-pentadiene are likely to be ruled out, because their ionization energies of 8.24 and 8.26 eV are below the observed threshold in the flame-sampled PIE curve. In addition, 1,5-hexadiene (IE = 9.27 eV) is a likely candidate to be present in the flame. This isomer can be formed either through ring-opening of the cyclohexyl radical followed by H-atom loss/abstraction, or by ring-opening of the 1-methyl-cyclohex-4-yl radical and subsequent β-scission abstracting the methyl group. It is notable that the flame-sampled PIE curve in Fig. 12 suggests equivalent mole fractions of the 1,3- and 1,5-hexadiene isomers at this position in the flame. The larger mole fraction of cyclohexene is probably a consequence of the unimolecular dissociation of the fuel forming cyclohexyl radicals.

Experimental mole fraction profiles for cyclohexene and the lumped 1,3-dienes are provided in Fig. 13. Modeled profiles for cyclohexene and 1,3-hexadiene are also included. The experimental 1,3-dienes mole fraction is evaluated at 8.8 eV. The cyclohexene mole fraction is then evaluated at 9 eV after correcting for contributions to the ion signal from the 1,3-dienes. In a similar fashion the mole fraction profile for 1,5-hexadiene (not shown) is evaluated at 9.7 eV, and a comparison of the 1,5-hexadiene mole fraction profile with that of the 1,3-dienes confirms the equivalent mole fractions suggested by the PIE curve (see Fig. 12).

The flame sampled PIE curve for *m/z* = 80 shown in Fig. 14 permits unambiguous identification of 1,3-cyclohexadiene and suggests the possible presence of the 1,4-isomer. A lack of PIE data for other isomers prevents us from explicitly identifying other, possibly linear or branched isomers. Experimental mole fraction profiles for 1,3-cyclohexadiene are provided in Fig. 15. Also included in the figure are the predicted mole fraction profiles for 1,3- and 1,4-cyclohexadiene and 1,3,5-hexatriene. While the model predicts an increased amount of 1,3,5-hexatriene under fuel-rich conditions, the stoichiometric and fuel-rich PIE curves for *m/z* = 80 are identical suggesting similar distributions of isomers in these flames.

An indicator of the relative importance of the dehydrogenation pathway compared to pathways involving small radical chemistry (e.g., the propargyl+propargyl reaction) is the fulvene-to-benzene ratio. For example, larger amounts of fulvene are observed in flames of allene and propyne in which the propargyl+propargyl reaction dominates ring formation.[41,42] On the other hand, in a stoichiometric cyclohexane flame only small amounts of fulvene were detected and most of the benzene was formed through sequential dehydrogenation processes.[16] Though anticipated to be short-lived in the flame due to H atom-assisted conversion to benzene,[43] a small contribution from fulvene to the ion signal at *m/z* = 78 is observed in Flames A and C as shown in Fig. 16. Contrary to the result of Li *et al.,*[18] the flame-sampled PIE curves at *m/z* = 78 for Flames A and C in this work are nearly identical, suggesting that the fulvene-to-benzene ratio in the MCH flames is not heavily dependent on the equivalence ratio. Additional evidence of this finding comes from a comparison of the peak experimental mole fractions in which a similar fulvene-to-benzene ratio is observed for Flame A and Flame C. The small amount of fulvene in this flame is an indicator that under the current condition benzene is mainly formed through dehydrogenation of the cyclohexyl radical, initially formed readily from the fuel.

Experimental and modeled benzene mole fraction profiles are shown for all flames in Fig. 17 along with scaled experimental fulvene mole fractions for Flames A and C. An experimental mole fraction profile for fulvene in Flame B could not be obtained due to poor signal quality for the low concentration species in the lower energy burner scans. The modeled fulvene profile is also omitted to avoid convoluting the figure. As can be expected, the largest amount of benzene is measured in Flame C, while, in spite of the large difference in equivalence ratio, the measured benzene mole fractions in Flames A and B are quite similar. This can be attributed to Flame B having a higher temperature, which has been shown to reduce not only the soot volume fraction in premixed flames but also the mole fractions of aromatics.[44,45] In addition, while the higher temperature of Flame B may lead to a relatively larger amount of MCH consumed via dissociation yielding cyclohexyl + CH_3, the results for toluene discussed above indicated that subsequent H-abstraction steps may be overshadowed by ring-opening reactions resulting in less rapid production of benzene by sequential H-abstraction from the cyclohexyl radical. It is also interesting to note that even though Flame C yields the largest benzene mole fraction, Flame A has the largest peak cyclohexene and cyclohexadiene mole fractions. This result provides further evidence that MCH dissociation leading to the cyclohexyl radical is more significant in the stoichiometric flame, which correlates to a relative reduction in the rates of the subsequent H-abstraction reactions leading ultimately to benzene.

The experimental and modeled peak benzene mole fractions are all within a factor of approx. two and, except for the disparity near the burner surface, the profile shapes and positions compare reasonably well. As mentioned previously, the experimental uncertainty in the mole fraction profiles can be as large as a factor of two, thus the model's performance with respect to

benzene is good. Nevertheless, Flame B is predicted to have the largest benzene mole fraction of the three flames studied which conflicts with the experimental results.

Recalling that the modeled 1,3-cyclohexadiene profiles for Flames B and C are low by factors of approx. 10 and 20, respectively, it is possible that correct predictions of this species would bring the modeled benzene trends for Flames B and C into better agreement with experiment. However, such a change would likely result in an overprediction of the benzene mole fraction for Flame B. Another possible explanation could be related to the rates and temperature dependencies of benzene oxidation reactions. Thus, in addition to improving rate parameters for the dehydrogenation reactions from cyclohexyl to benzene, further analysis of the other benzene production and destruction reactions should also be considered for future kinetic models.

Conclusions

A detailed experimental analysis of MCH decomposition leading to stable C_7 and C_6 species is performed in three low-pressure premixed flames using molecular beam mass spectrometry. Evidence for the presence of several straight-chain, branched, and cyclic isomers having the general formulas C_7H_{12}, C_7H_{10}, C_6H_{12}, and C_6H_{10} is shown and the relevant MCH decomposition pathways leading to these species are discussed. When appropriate, newly calculated ionization energies are provided to aid in species identification via photoionization efficiency curves. An analysis of the three MCH consumption pathways (H-abstraction, isomerization, and dissociation) indicates that flame structures having larger temperature gradients and/or higher maximum temperatures result in a relative increase in the percentage of MCH consumed via isomerization and dissociation. Relatively large toluene mole fractions are

ACS Paragon Plus Environment

also observed in these flames, which highlight the importance of sequential H-abstraction, the propensity for MCH flames to soot, and the potential toxicity of MCH as a significant component of real fuels. Benzene is also observed in relatively large amounts and a comparison of the cyclohexene, cyclohexadiene, and benzene mole fraction profiles provides additional evidence that the relative contributions from the three MCH consumption pathways depend on flame structure. Small and similar relative amounts of fulvene observed under stoichiometric and fuel-rich conditions suggest that the role of small-radical-chemistry leading to benzene in these flames may be limited, and that sequential H-abstraction from the cyclohexyl radical could indeed be a dominant benzene formation pathway. Several quantitative experimental mole fraction profiles are compared with modeled results providing a benchmark for the most current MCH specific mechanism of Pitz *et al.*[3] Modeled results consistently underpredict the stable C_7 species indicating a need for improved rate coefficients, while predictions for the cyclic C_6 species as well as 1,3-pentadiene and isoprene fare significantly better. An updated version of the MCH combustion chemistry model used in this work is currently under development and will be presented in future work.

Acknowledgments

This work is supported by the U.S Department of Energy, Office of Basic Energy Sciences under the Single Investigator Small Group Research (SISGR, Grant No. DE-SC0002619) with Angela Violi as the principle investigator. The measurements are performed within the "Flame Team" collaboration at the Advanced Light Source (ALS) of the Lawrence Berkeley National Laboratory. We thank Terrill Cool, Patrick Oßwald, and Wenjun Li for valuable contributions to the data collection. We also acknowledge the expert technical

assistance of Paul Fugazzi. The Advanced Light Source is supported by the Director, Office of Science, Office of Basic Energy Sciences, of the U.S. Department of Energy under Contract No. DE-AC02-05CH11231. The work at LLNL was performed under the auspices of the U.S. Department of Energy by Lawrence Livermore National Laboratory under Contract DE-AC52-07NA27344. Sandia is a multi-program laboratory operated by Sandia Corporation, a Lockheed Martin Company, for the National Nuclear Security Administration under contract DE-AC04-94-AL85000.

References:

(1) Pitz, W. J.; Mueller, C. J. *Progr. Energy Combust. Sci.* **2011,** *37,* 330-350.

(2) Bieleveld, T.; Frassoldati, A.; Cuoci, A.; Faravelli, T.; Ranzi, E.; Niemann, U.; Seshadri, K. *Proc. Combust. Inst.* **2009,** *32,* 493-500.

(3) Pitz, W. J.; Naik, C. V.; Mhaolduin, T. N.; Westbrook, C. K.; Curran, H. J.; Orme, J. P.; Simmie, J. M. *Proc. Combust. Inst.* **2007,** *31,* 267-275.

(4) Granata, S.; Faravelli, T.; Ranzi, E. *Combust. Flame* **2003,** *132,* 533-544.

(5) Orme, J. P.; Curran, H. J.; Simmie, J. M. *J. Phys. Chem. A* **2006,** *110,* 114-131.

(6) A high-temperature chemical kinetic model of n-alkane (up to n-dodecane), cyclohexane, and methyl-, ethyl-, n-propyl and n-butyl-cyclohexane oxidation at high temperatures, JetSurF version 2.0, September 19, 2010.

(7) Zeppieri, S.; Brezinsky, K.; Glassman, I. *Combust. Flame* **1997,** *108,* 266-286.

(8) Mittal, G.; Sung, C. J. *Combust. Flame* **2009,** *156,* 1852-1855.

(9) Ji, C. S.; Dames, E.; Sirjean, B.; Wang, H.; Egolfopoulos, F. N. *Proc. Combust. Inst.* **2011,** *33,* 971-978.

(10) Hong, Z. K.; Lam, K. Y.; Davidson, D. F.; Hanson, R. K. *Combust. Flame* **2011,** *158,* 1456-1468.

(11) Vanderover, J.; Oehlschlaeger, M. A. *Int. J. Chem. Kin.* **2009,** *41,* 82-91.

(12) Vasu, S. S.; Davidson, D. F.; Hanson, R. K. *Combust. Flame* **2009,** *156,* 736-749.

(13) Vasu, S. S.; Davidson, D. F.; Hong, Z.; Hanson, R. K. *Energy Fuels* **2009,** *23,* 175-185.

(14) McEnally, C. S.; Pfefferle, L. D. *Proc. Combust. Inst.* **2005,** *30,* 1425-1432.

(15) Zhang, H. R.; Huynh, L. K.; Kungwan, N.; Yang, Z.; Zhang, S. *J. Phys. Chem. A* **2007,** *111,* 4102-4115.

(16) Law, M. E.; Westmoreland, P. R.; Cool, T. A.; Wang, J.; Hansen, N.; Taatjes, C. A.; Kasper, T. *Proc. Combust. Inst.* **2007,** *31,* 565-573.

(17) Hansen, N.; Kasper, T.; Yang, B.; Cool, T. A.; Li, W.; Westmoreland, P. R.; Osswald, P.; Kohse-Höinghaus, K. *Proc. Combust. Inst.* **2011,** *33,* 585-592.

(18) Li, W.; Law, M. E.; Westmoreland, P. R.; Kasper, T.; Hansen, N.; Kohse-Höinghaus, K. *Combust. Flame* **2011,** *158,* 2077-2089.

(19) Cool, T. A.; McIlroy, A.; Qi, F.; Westmoreland, P. R.; Poisson, L.; Peterka, D. S.; Ahmed, M. *Rev. Sci. Instr.* **2005,** *76,* 094102.

(20) Cool, T. A.; Nakajima, K.; Taatjes, C. A.; McIlroy, A.; Westmoreland, P. R.; Law, M. E.; Morel, A. *Proc. Combust. Inst.* **2005,** *30,* 1681-1688.

(21) Hansen, N.; Cool, T. A.; Westmoreland, P. R.; Kohse-Höinghaus, K. *Progr. Energy Combust. Sci.* **2009,** *35,* 168-191.

(22) Oßwald, P.; Struckmeier, U.; Kasper, T.; Kohse-Höinghaus, K.; Wang, J.; Cool, T. A.; Hansen, N.; Westmoreland, P. R. *J. Phys. Chem. A* **2007,** *111,* 4093-4101.

(23) Wang, J.; Yang, B.; Cool, T. A.; Hansen, N.; Kasper, T. *Int. J. Mass Spectrom.* **2008,** *269,* 210-220.

(24) Yang, B.; Wang, J.; Cool, T. A.; Hansen, N.; Skeen, S. A.; Osborn, D. L. *Int. J. Mass Spectrom.* **2011,** accepted (doi:10.1016/j.ijms.2011.09.006).

(25) Zhou, Z. Y.; Zhang, L. D.; Xie, M. F.; Wang, Z. D.; Chen, D. N.; Qi, F. *Rapid Commun. Mass Sp.* **2010,** *24,* 1335-1342.

(26) Koizumi, H. *J. Chem. Phys.* **1991,** *95,* 5846-5852.

(27) Hansen, N.; Harper, M. R.; Green, W. H. *Phys. Chem. Chem. Phys.* **2011,** accepted (DOI:10.1039/C1CP21663E).

(28) Hansen, N.; Klippenstein, S. J.; Miller, J. A.; Wang, J.; Cool, T. A.; Law, M. E.; Westmoreland, P. R.; Kasper, T.; Kohse-Höinghaus, K. *J. Phys. Chem. A* **2006,** *110,* 4376-4388.

(29) Hansen, N.; Klippenstein, S. J.; Taatjes, C. A.; Miller, J. A.; Wang, J.; Cool, T. A.; Yang, B.; Yang, R.; Wei, L. X.; Huang, C. Q.; Wang, J.; Qi, F.; Law, M. E.; Westmoreland, P. R. *J. Phys. Chem. A* **2006,** *110,* 3670-3678.

(30) Kasper, T.; Lucassen, A.; Jasper, A. W.; Li, W.; Westmoreland, P. R.; Kohse-Höinghaus, K.; Yang, B.; Wang, J.; Cool, T. A.; Hansen, N. *Z. Phys. Chem.* **2011,** *submitted,*

(31) Hansen, N.; Klippenstein, S. J.; Westmoreland, P. R.; Kasper, T.; Kohse-Höinghaus, K.; Wang, J.; Cool, T. A. *Phys. Chem. Chem. Phys.* **2008,** *10,* 366-374.

(32) Kiefer, J. H.; Gupte, K. S.; Harding, L. B.; Klippenstein, S. J. *J. Phys. Chem. A* **2009,** *113,* 13570-13583.

(33) Chemkin-PRO, Reaction Design, San Diego, 2010.

(34) Struckmeier, U.; Oßwald, P.; Kasper, T.; Böhling, L.; Heusing, M.; Köhler, M.; Brockhinke, A.; Kohse-Höinghaus, K. *Z. Phys. Chem.* **2009,** *223,* 503-537.

(35) "Ionization Energy Evaluation" by S.G. Lias in NIST Chemistry WebBook, NIST Standard Reference Database Number 69, Eds. P.J. Linstrom and W.G. Mallard, National Institute of Standards and Technology, Gaithersburg MD, 20899, http://webbook.nist.gov, (retrieved August 4, 2011).

(36) Yang, X.; Jasper, A. W.; Giri, B. R.; Kiefer, J. H.; Tranter, R. S. *Physical Chemistry Chemical Physics* **2011,** *13,* 3686-3700.

(37) Dames, E.; Krylov, A.; Wang, H. *Proceedings of the US National Technical Meeting of the Combustion Institute* **2011,** Paper 1B16.

(38) Brown, T. C.; King, K. D. *Int. J. Chem. Kin.* **1989,** *21,* 251-266.

(39) Hansen, N.; Li, W.; Law, M. E.; Kasper, T.; Westmoreland, P. R.; Yang, B.; Cool, T. A.; Lucassen, A. *Phys. Chem. Chem. Phys.* **2010,** *12,* 12112-12122.

(40) Astrup, E. E.; Bock, H.; Wittel, K.; Heimbach, P. *Acta Chem. Scand. A* **1975,** *29,* 827-832.

(41) Hansen, N.; Miller, J. A.; Taatjes, C. A.; Wang, J.; Cool, T. A.; Law, M. E.; Westmoreland, P. R. *Proc. Combust. Inst.* **2007,** *31,* 1157-1164.

(42) Hansen, N.; Miller, J. A.; Westmoreland, P. R.; Kasper, T.; Kohse-Höinghaus, K.; Wang, J.; Cool, T. A. *Combust. Flame* **2009,** *156,* 2153-2164.

(43) Melius, C. F.; Colvin, M. E.; Marinov, N. M.; Pit, W. J.; Senkan, S. M. *Proc. Combust. Inst.* **1996,** *26,* 685-692.

(44) Ciajolo, A.; D'Anna, A.; Barbella, R.; Tregrossi, A.; Violi, A. *Symposium (International) on Combustion* **1996,** *26,* 2327-2333.

(45) Haynes, B. S.; Wagner, H. G. *Progress in Energy and Combustion Science* **1981,** *7,* 229-273.

List of Figures

Scheme 1. Conceivable methylcyclohexane consumption reactions: (1) H-abstraction reactions forming isomeric C_7H_{13} radicals, (2) unimolecular dissociation forming cyclohexyl radicals, and (3) ring-opening reactions forming 1- and 2-heptene, or 2-, 3-, 4-, and 5-methyl-1-hexene.

Scheme 2. Formation of various C_7H_{12} isomers from the initially formed C_7H_{13} radicals through H-abstraction reactions and ring-opening followed by H-abstraction.

Scheme 3. Formation of various C_6H_{12} isomers from the initially formed C_7H_{13} radicals through β-scission and methyl radical addition.

Figure 1. Experimental (symbols) and modeled (lines) mole fraction profiles as function of distance from the burner surface for the major species in flames A-C. The experimental temperature profiles are also included.

Figure 2. (a) Flame-sampled photoionization efficiency curves for m/z = 98 (C_7H_{14}). Evidence for the isomerization reaction of MCH to heptenes and/or methyl-substituted hexene isomers is provided. (b) Experimental (connected symbols) and modeled (lines) mole fraction profiles for the linear and branched C_7H_{14} alkenes in Flames A and C.

Figure 3. Zero point inclusive CASPT2/cc-pVDZ potential energy diagram for MCH isomerization and dissociation.

Figure 4. Flame-sampled photoionization efficiency curve for *m/z* = 96 (C_7H_{12}).

Figure 5. Experimental (connected symbols) and modeled (lines) mole fraction profiles for *m/z* = 96 (C_7H_{12}) species. The isomers are partially separated. The modeled profiles are multiplied by a factor of 10.

Figure 6. Flame-sampled PIE curve for *m/z* = 84 (C_6H_{12}). The known PIE curves for 1- and 2-hexene and cyclohexane are also shown.

Figure 7. Flame-sampled photoionization efficiency curve for *m/z* = 68. The presence of 1,3-pentadiene and isoprene are confirmed. Cyclopentene and 1,4-pentadiene are also possible isomers. No obvious indication of cyclopentene is apparent in the flame sampled PIE curve; however the change in slope slightly above 9.5 eV suggests ion signal from 1,4-pentadiene may be present.

Figure 8. Experimental (connected symbols) and modeled (lines) mole fraction profiles for 1,3-pentadiene and isoprene. As necessary, the modeled profiles have been scaled to yield better agreement with the experimental data.

Figure 9. Flame-sampled photoionization efficiency curve for *m/z* = 94 (C_7H_{10}). The ionization energies of conceivably detectable combustion intermediates are indicated. Ion signal observed at the lowest experimental photon energy (8.1 eV) indicates the possible presence of 1,3,5-heptatriene, 1-methyl-1,3-cyclohexadiene and/or 2-methyl-1,3-cyclohexadiene.

Figure 10. Experimental mole fraction profiles for *m/z* = 94 (C_7H_{10}) (connected symbols) are compared with flame-modeling predictions (lines). The modeled results are multiplied by a factor of 100.

Figure 11. Mole fraction profiles of toluene for Flames A-C. Although the modeled (lines) peak position and profile shapes agree well with the experimental (connected symbols) results, the peak value is underpredicted by a factor as large as 100. Also included are experimentally determined toluene profile of a stoichiometric cyclohexane flame (top) (Ref. 16) and a fuel-rich 1-hexene flame (bottom) (Ref. 39).

Figure 12. Flame-sampled PIE curve for *m/z* = 82 (C_6H_{10}). The presence of cyclohexene, 1,3-, and 1,5- hexadiene is evident by comparison with cold-flow PIE curves of these compounds.

Figure 13. Experimental (symbols) and modeled (lines) mole-fraction profiles for 1,3-hexadiene and cyclohexene. The modeled profiles have been scaled as necessary to yield better agreement with experiment.

Figure 14. The flame-sampled photoionization efficiency (PIE) curve is compared with the cold-flow PIE curve of 1,3-cyclohexadiene. The presence of both 1,3- and 1,4-cyclohexadiene can be confirmed.

Figure 15. Experimental (connected symbols) mole fraction profiles for 1,3-cyclohexadiene and modeled (lines) mole fraction profiles for 1,3-cyclohexadiene, 1,4-cyclohexadiene, and 1,3,5-hexatriene. The modeled profiles for Flames A, B, and C are scaled by factors of 4, 10, and 20, respectively.

Figure 16. Flame-sampled photoionization efficiency curve for *m/z* = 78. Although weak, the presence of fulvene is established.

Figure 17. Experimental (open symbols) and modeled (lines) mole fraction profiles for benzene. Experimental fulvene mole fractions (closed symbols) for Flames A and C are also included and have been multiplied by a factor of 30.

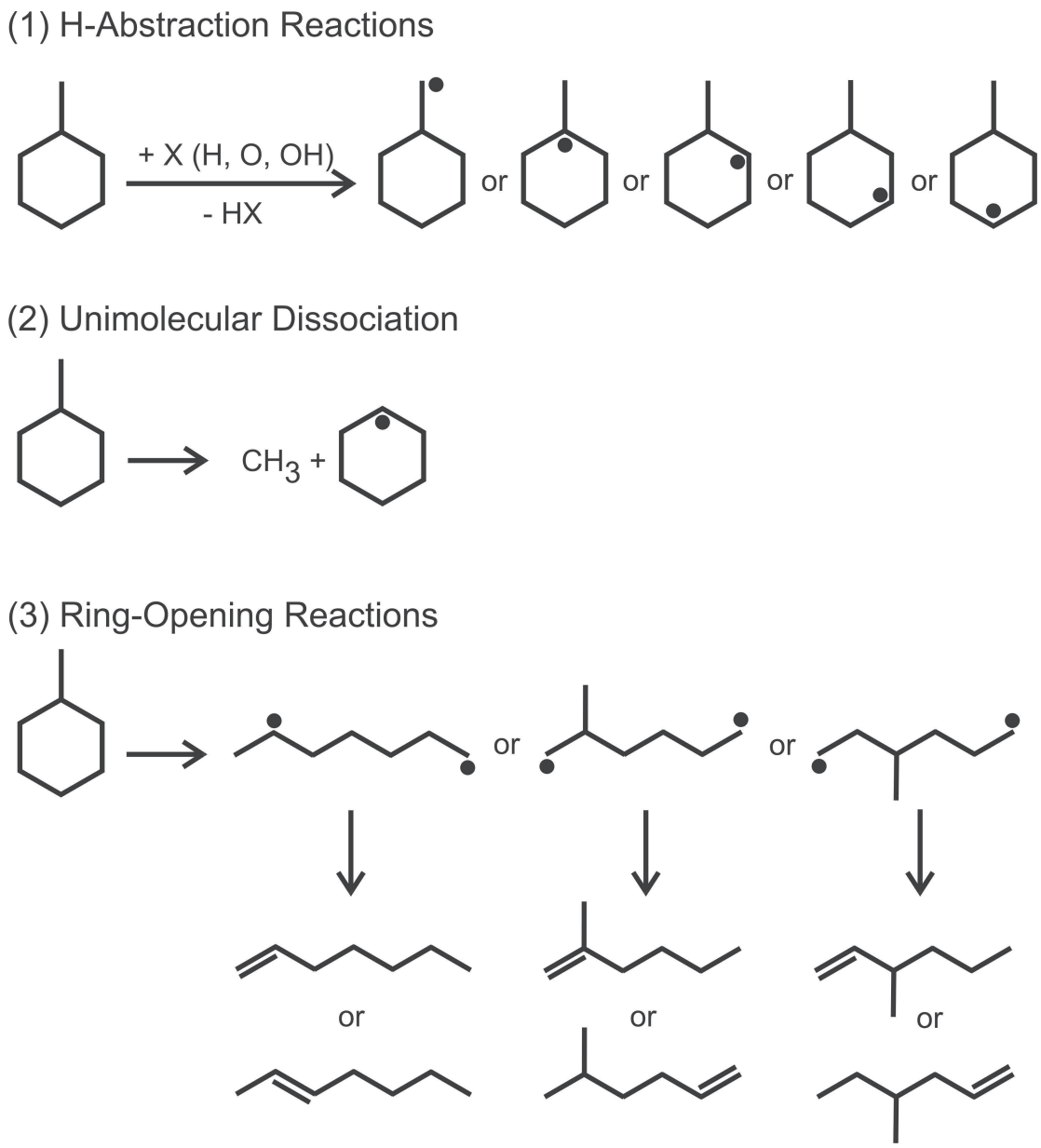
(1) H-Abstraction Reactions
+ X (H, O, OH)
- HX
or
or
or
or
(2) Unimolecular Dissociation
CH_3 +
(3) Ring-Opening Reactions
or
or
or
or
or

Scheme 1

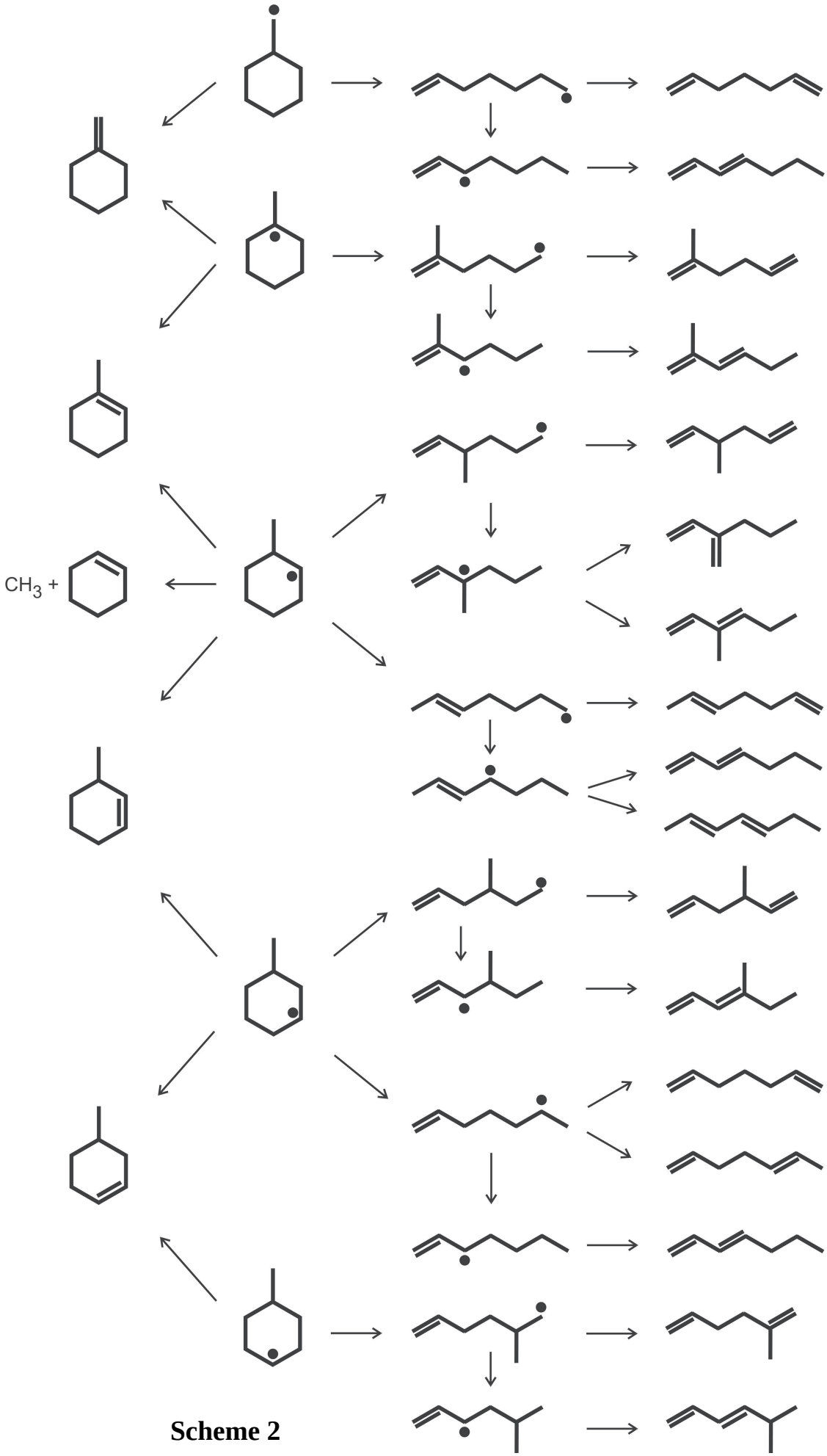

Scheme 2

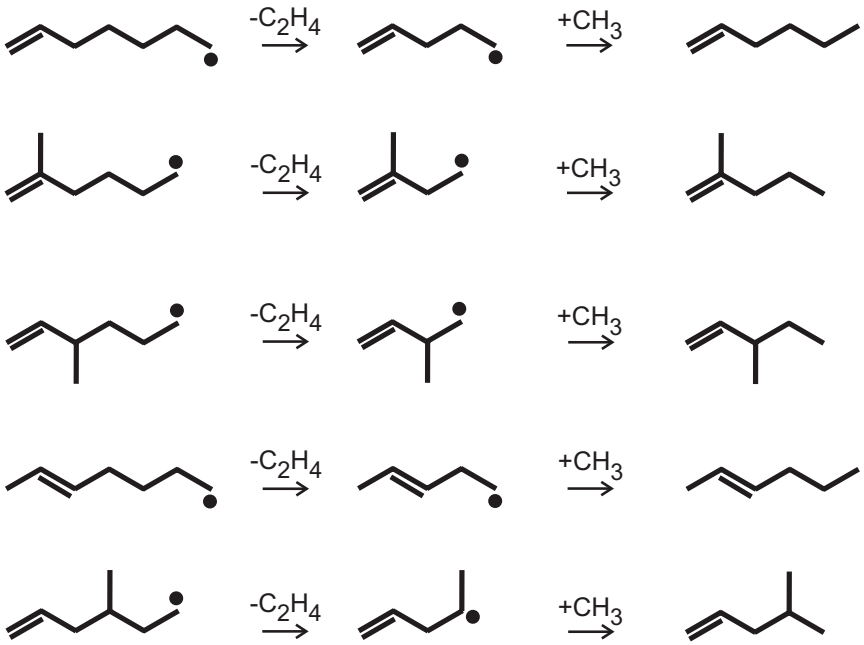

Scheme 3

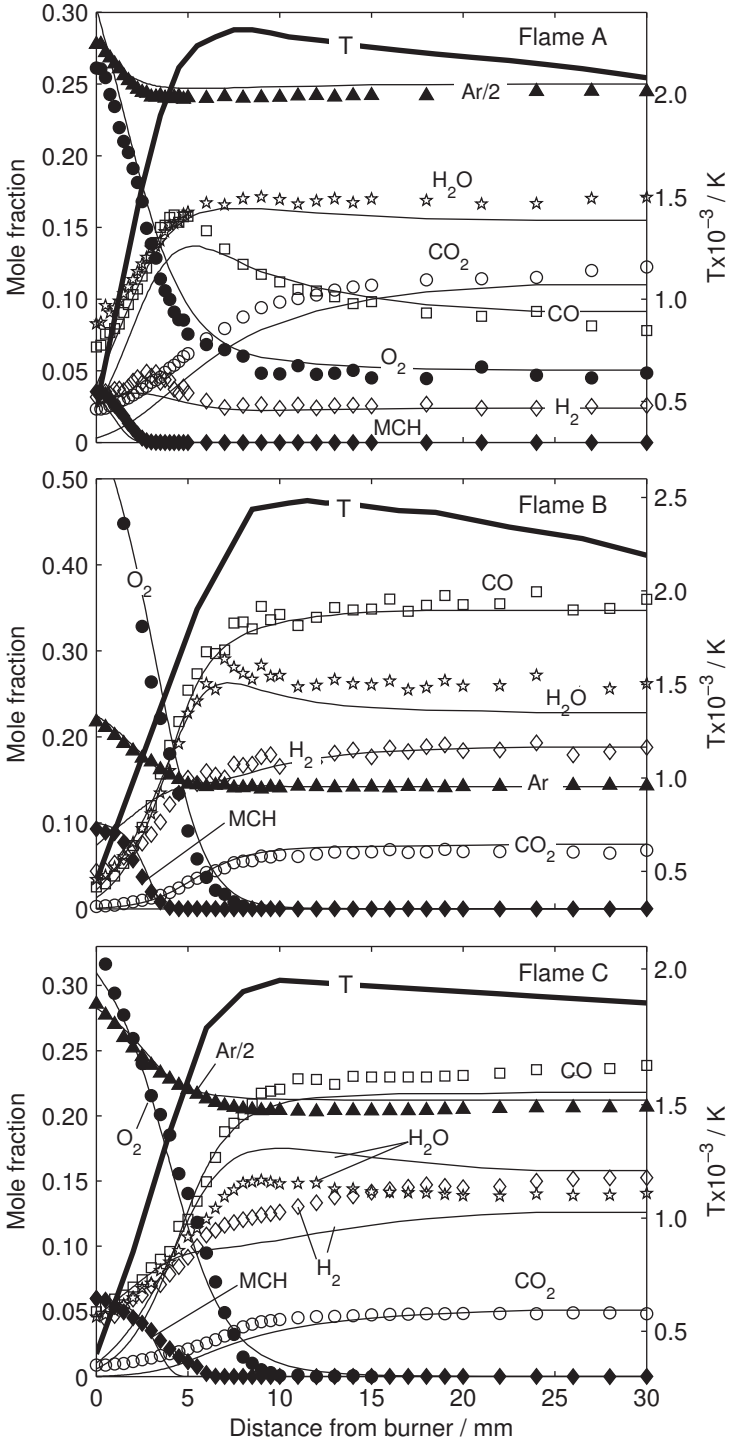
Flame A
T
Ar/2
H_2O
CO_2
CO
O_2
H_2
MCH
Flame B
T
O_2
CO
H_2O
H_2
Ar
MCH
CO_2
Flame C
T
Ar/2
CO
O_2
H_2O
H_2
MCH
CO_2
Mole fraction
$Tx10^{-3}$ / K
Distance from burner / mm

Figure 1

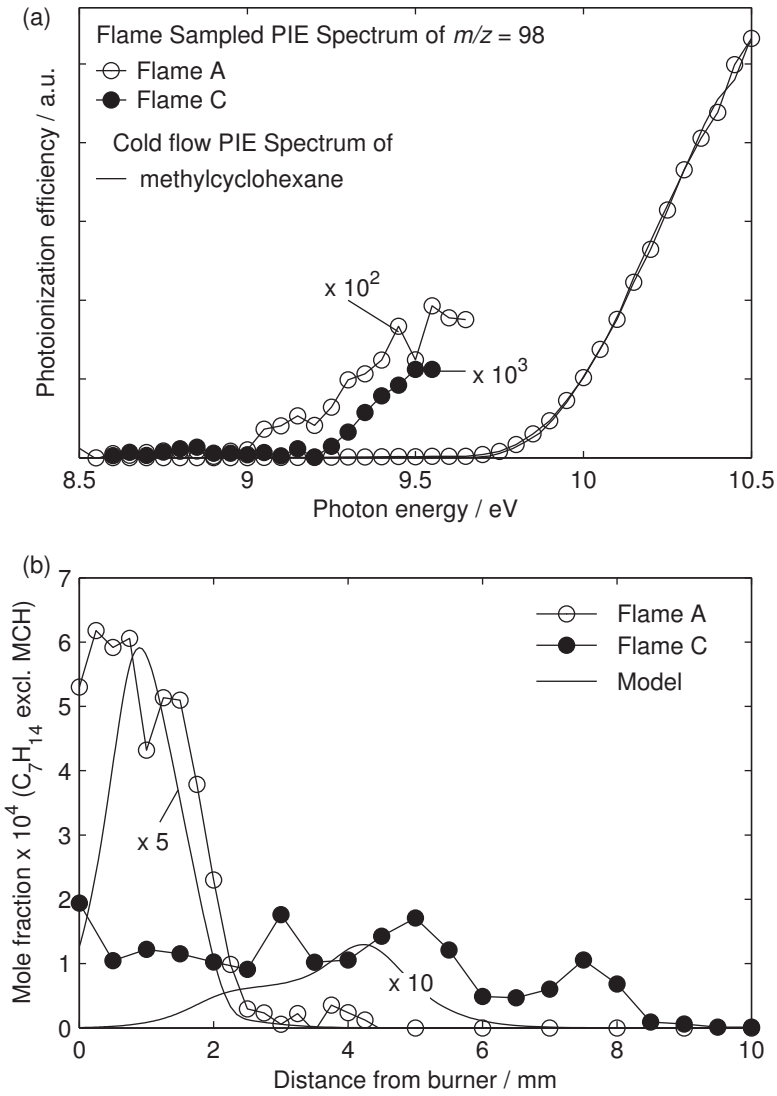
(a)
Flame Sampled PIE Spectrum of m/z = 98
Flame A
Flame C
Cold flow PIE Spectrum of
methylcyclohexane
x 10^2
x 10^3
Photoionization efficiency / a.u.
8.5
9
9.5
10
10.5
Photon energy / eV
(b)
Flame A
Flame C
Model
x 5
x 10
Mole fraction x 10^4 (C7H14 excl. MCH)
0
1
2
3
4
5
6
7
0
2
4
6
8
10
Distance from burner / mm

Figure 2

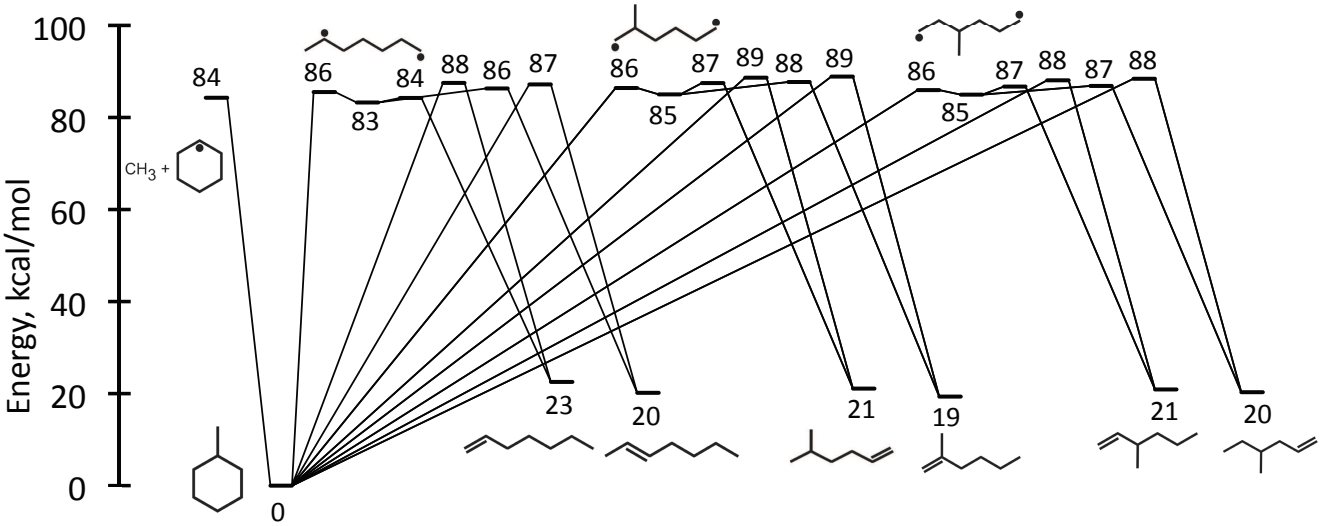
Energy, kcal/mol
100
80
60
40
20
0
CH3 +
84
0
86
83
84
88
86
87
23
86
85
87
20
89
88
89
21
86
85
87
19
88
87
21
88
20

Figure 3

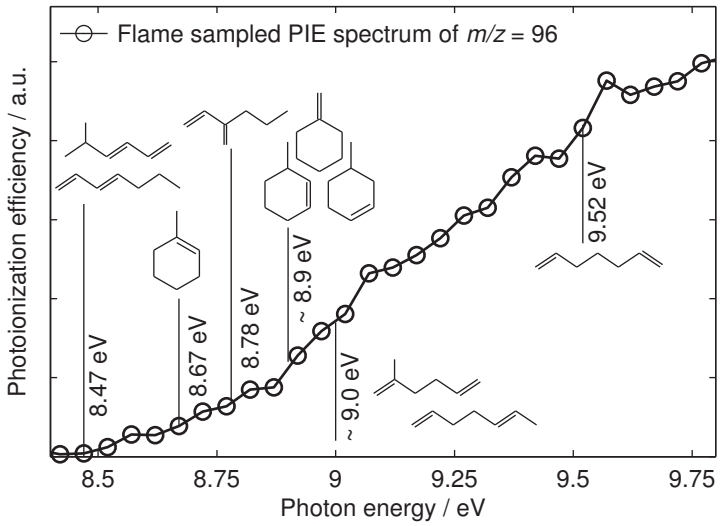
Flame sampled PIE spectrum of m/z = 96
Photoionization efficiency / a.u.
Photon energy / eV
8.5
8.75
9
9.25
9.5
9.75
8.47 eV
8.67 eV
8.78 eV
~ 8.9 eV
~ 9.0 eV
9.52 eV

Figure 4

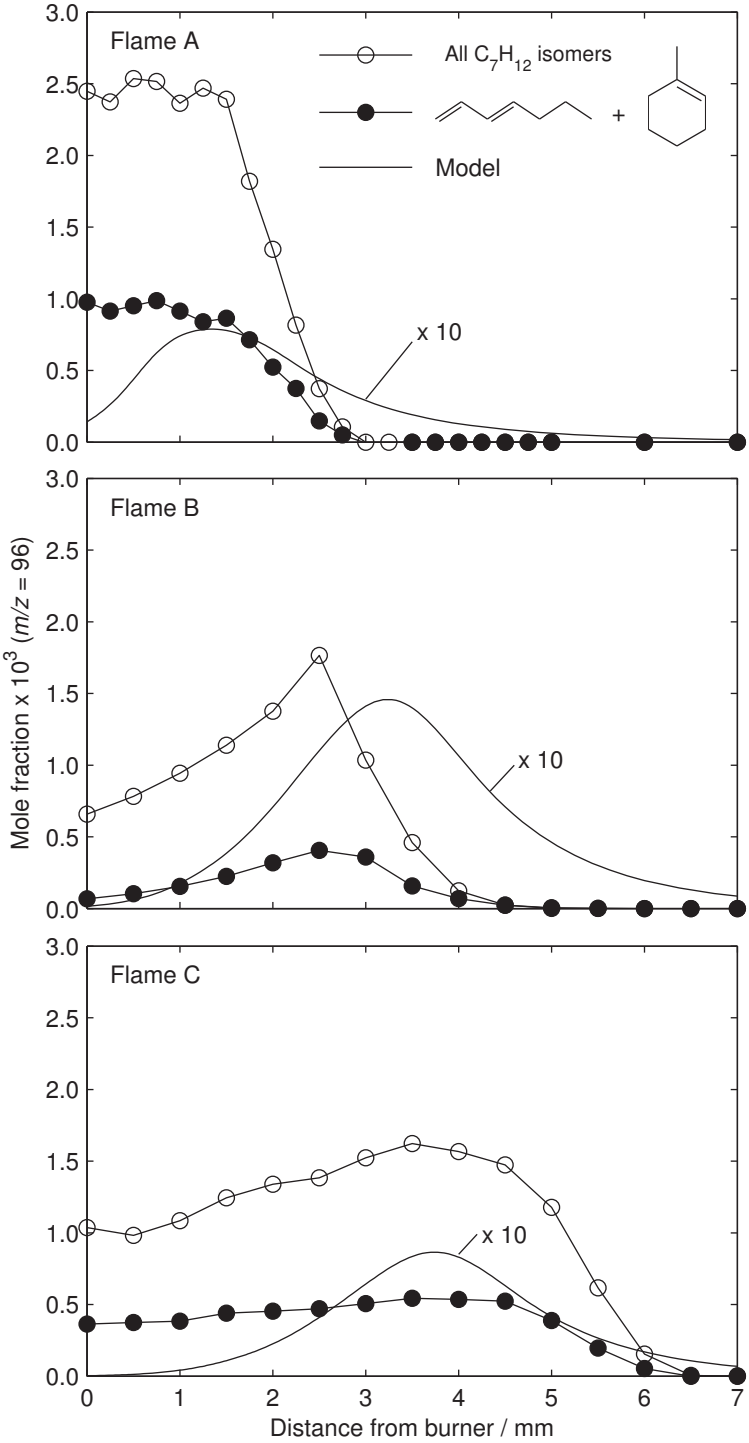
Flame A
All C7H12 isomers
+
Model
x 10
Flame B
x 10
Flame C
x 10
Mole fraction x 10^3 (m/z = 96)
Distance from burner / mm
0.0
0.5
1.0
1.5
2.0
2.5
3.0
0
1
2
3
4
5
6
7

Figure 5

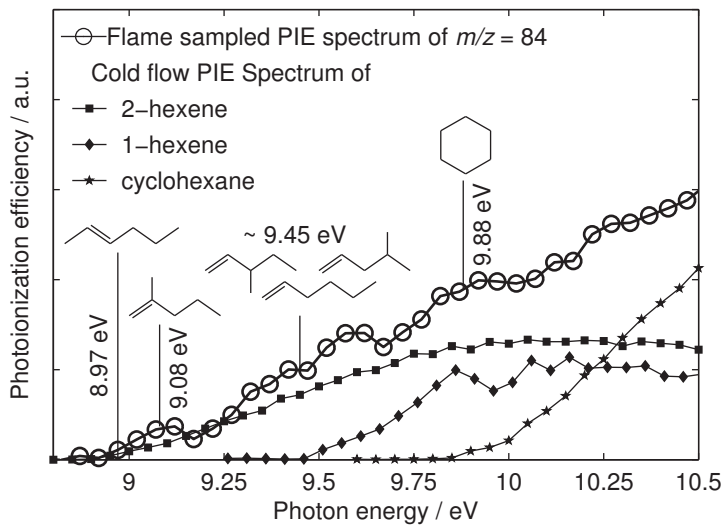
Flame sampled PIE spectrum of m/z = 84
Cold flow PIE Spectrum of
2–hexene
1–hexene
cyclohexane
~ 9.45 eV
9.88 eV
8.97 eV
9.08 eV
Photoionization efficiency / a.u.
9
9.25
9.5
9.75
10
10.25
10.5
Photon energy / eV

Figure 6

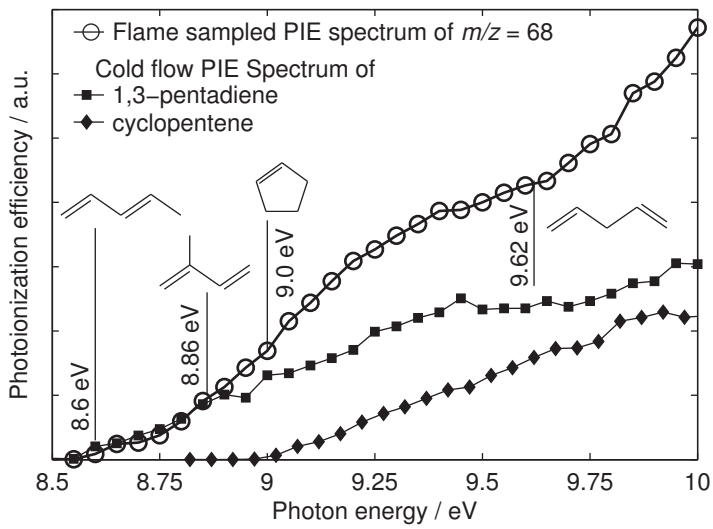
Flame sampled PIE spectrum of m/z = 68
Cold flow PIE Spectrum of
1,3–pentadiene
cyclopentene
8.6 eV
8.86 eV
9.0 eV
9.62 eV
Photoionization efficiency / a.u.
8.5
8.75
9
9.25
9.5
9.75
10
Photon energy / eV

Figure 7

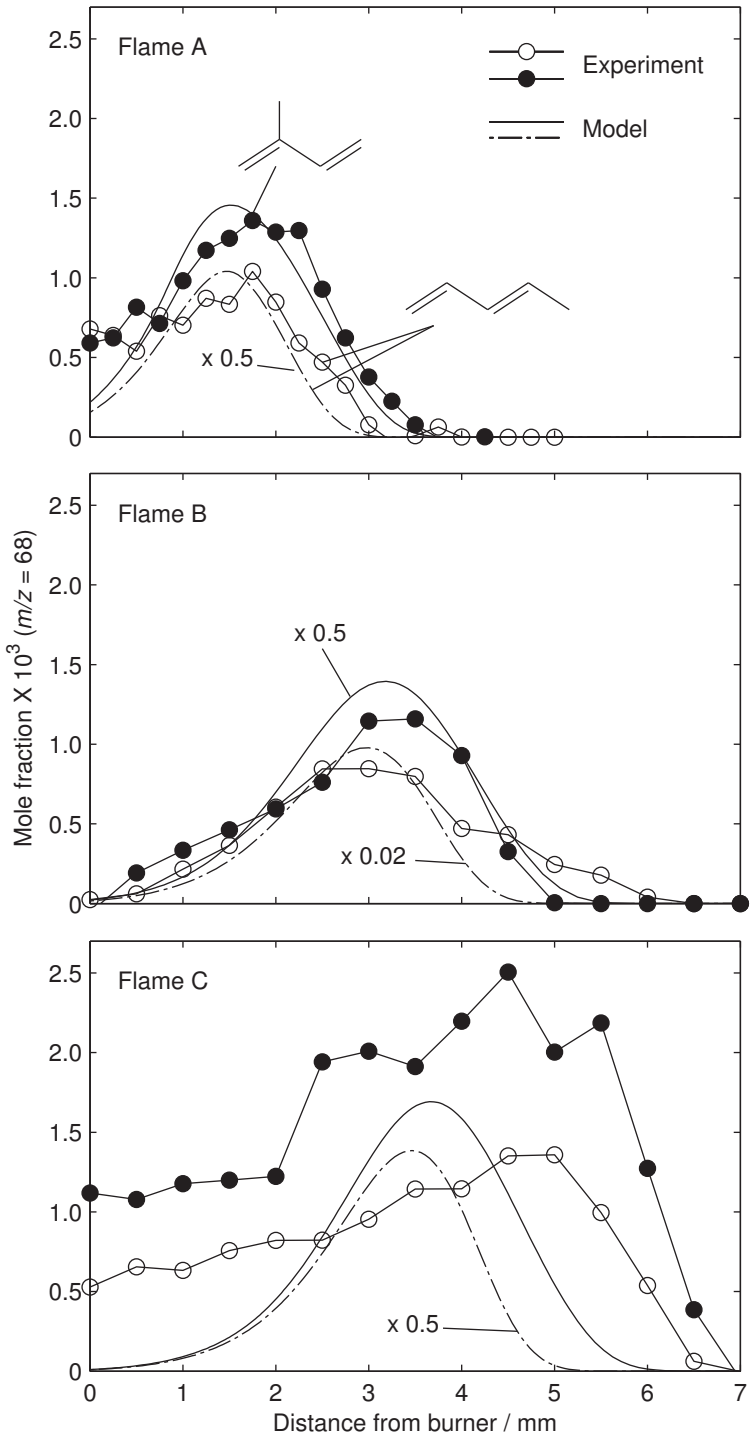
Flame A
Experiment
Model
x 0.5
Flame B
x 0.5
x 0.02
Flame C
x 0.5
Mole fraction X 10^3 (m/z = 68)
Distance from burner / mm
0
0.5
1.0
1.5
2.0
2.5
0
1
2
3
4
5
6
7

Figure 8

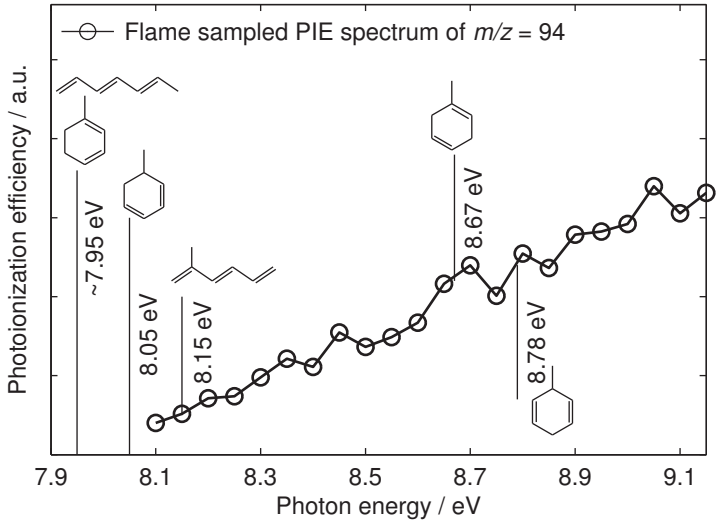
Flame sampled PIE spectrum of m/z = 94
Photoionization efficiency / a.u.
Photon energy / eV
7.9
8.1
8.3
8.5
8.7
8.9
9.1
~7.95 eV
8.05 eV
8.15 eV
8.67 eV
8.78 eV

Figure 9

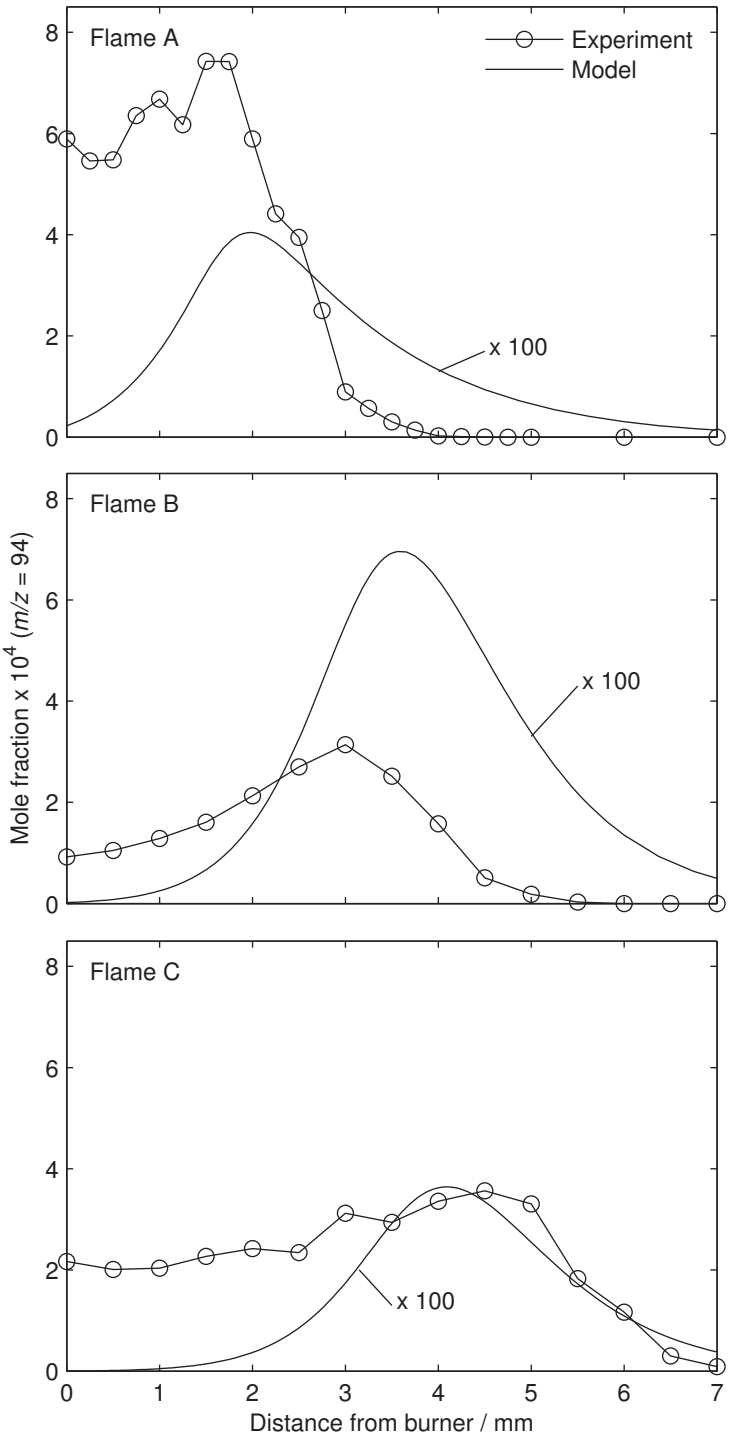
Flame A
Experiment
Model
x 100
Flame B
x 100
Flame C
x 100
Mole fraction x 10^4 (m/z = 94)
Distance from burner / mm
0
2
4
6
8
0
1
2
3
4
5
6
7

Figure 10

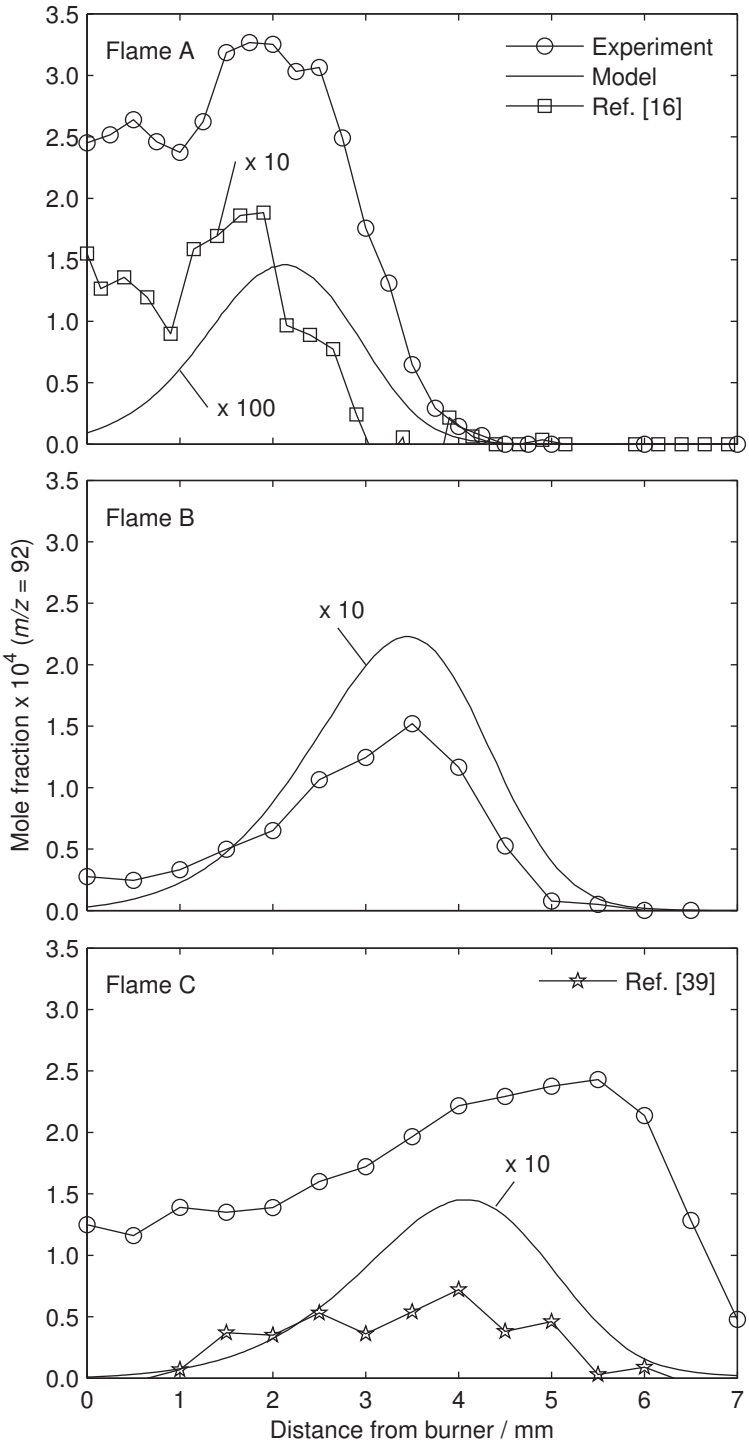
Flame A
Experiment
Model
Ref. [16]
x 10
x 100
Flame B
x 10
Flame C
Ref. [39]
x 10
Mole fraction x 10^4 (m/z = 92)
Distance from burner / mm
0.0
0.5
1.0
1.5
2.0
2.5
3.0
3.5
0
1
2
3
4
5
6
7

Figure 11

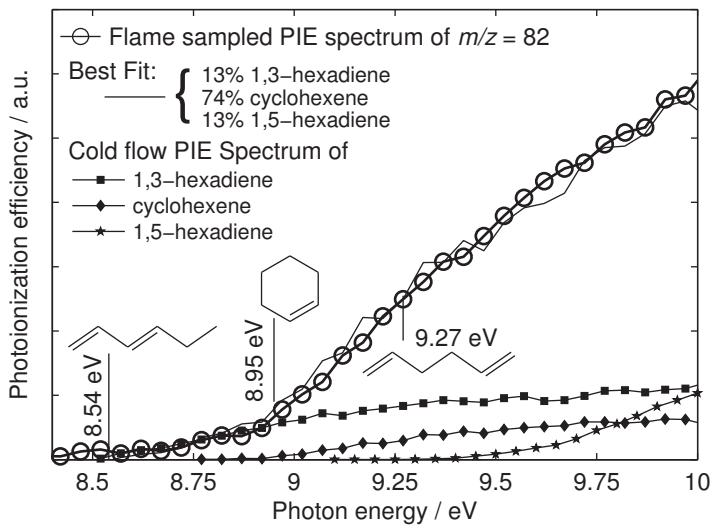
Flame sampled PIE spectrum of m/z = 82
Best Fit:
13% 1,3–hexadiene
74% cyclohexene
13% 1,5–hexadiene
Cold flow PIE Spectrum of
1,3–hexadiene
cyclohexene
1,5–hexadiene
8.54 eV
8.95 eV
9.27 eV
Photoionization efficiency / a.u.
8.5
8.75
9
9.25
9.5
9.75
10
Photon energy / eV

Figure 12

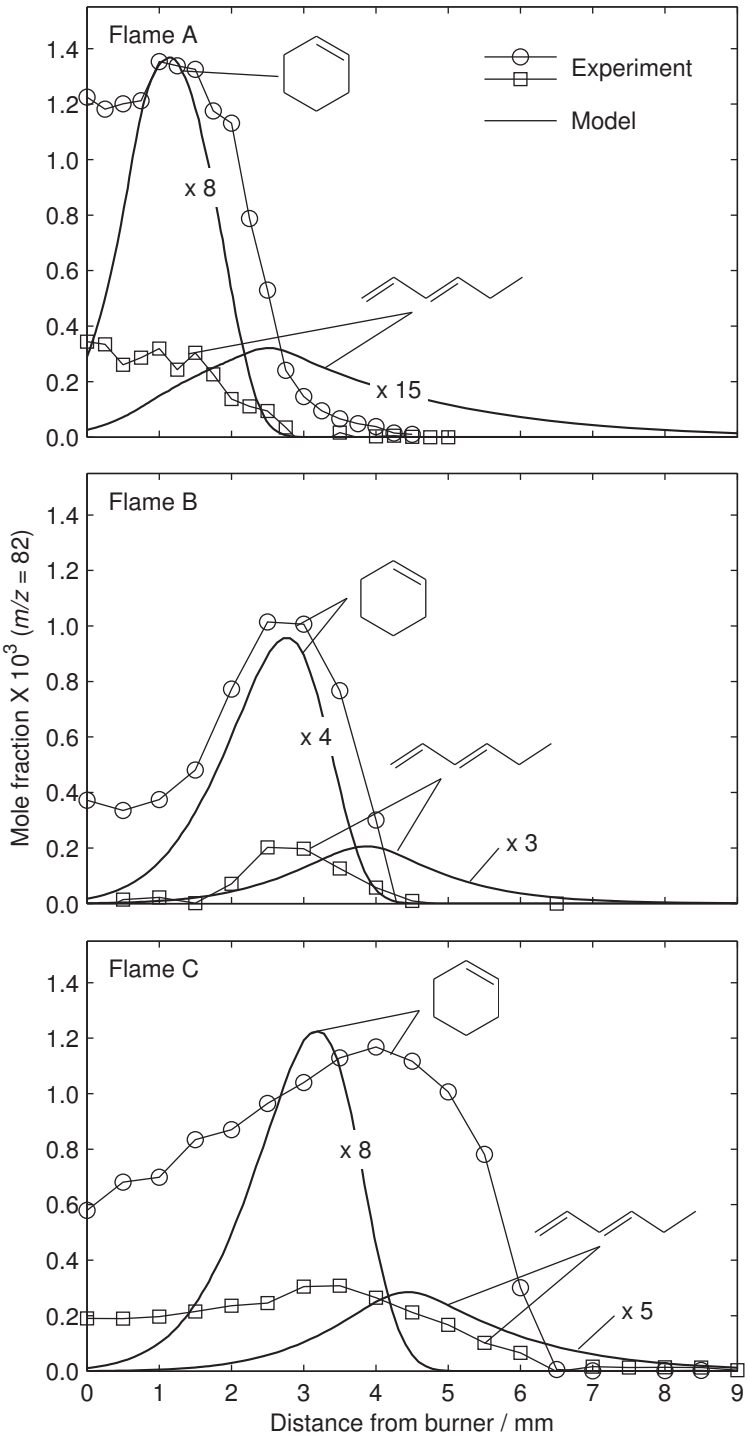
Flame A
Experiment
Model
x 8
x 15
Flame B
x 4
x 3
Flame C
x 8
x 5
Mole fraction X 10^3 (m/z = 82)
Distance from burner / mm
0.0
0.2
0.4
0.6
0.8
1.0
1.2
1.4
0
1
2
3
4
5
6
7
8
9

Figure 13

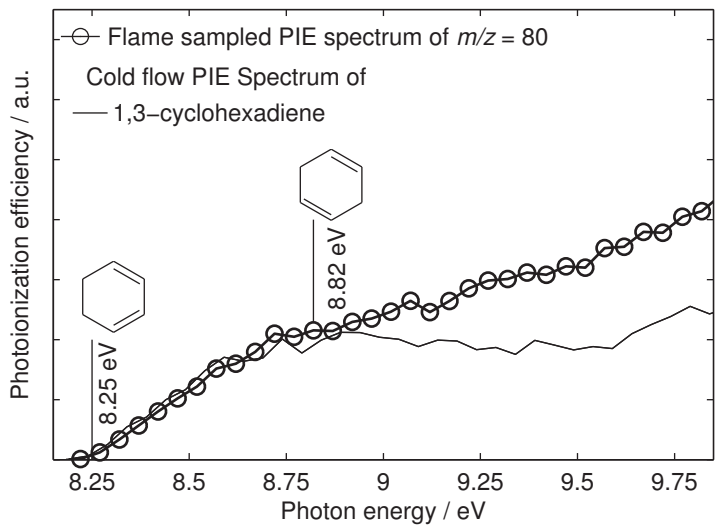
Flame sampled PIE spectrum of m/z = 80
Cold flow PIE Spectrum of
1,3–cyclohexadiene
8.25 eV
8.82 eV
Photoionization efficiency / a.u.
8.25
8.5
8.75
9
9.25
9.5
9.75
Photon energy / eV

Figure 14

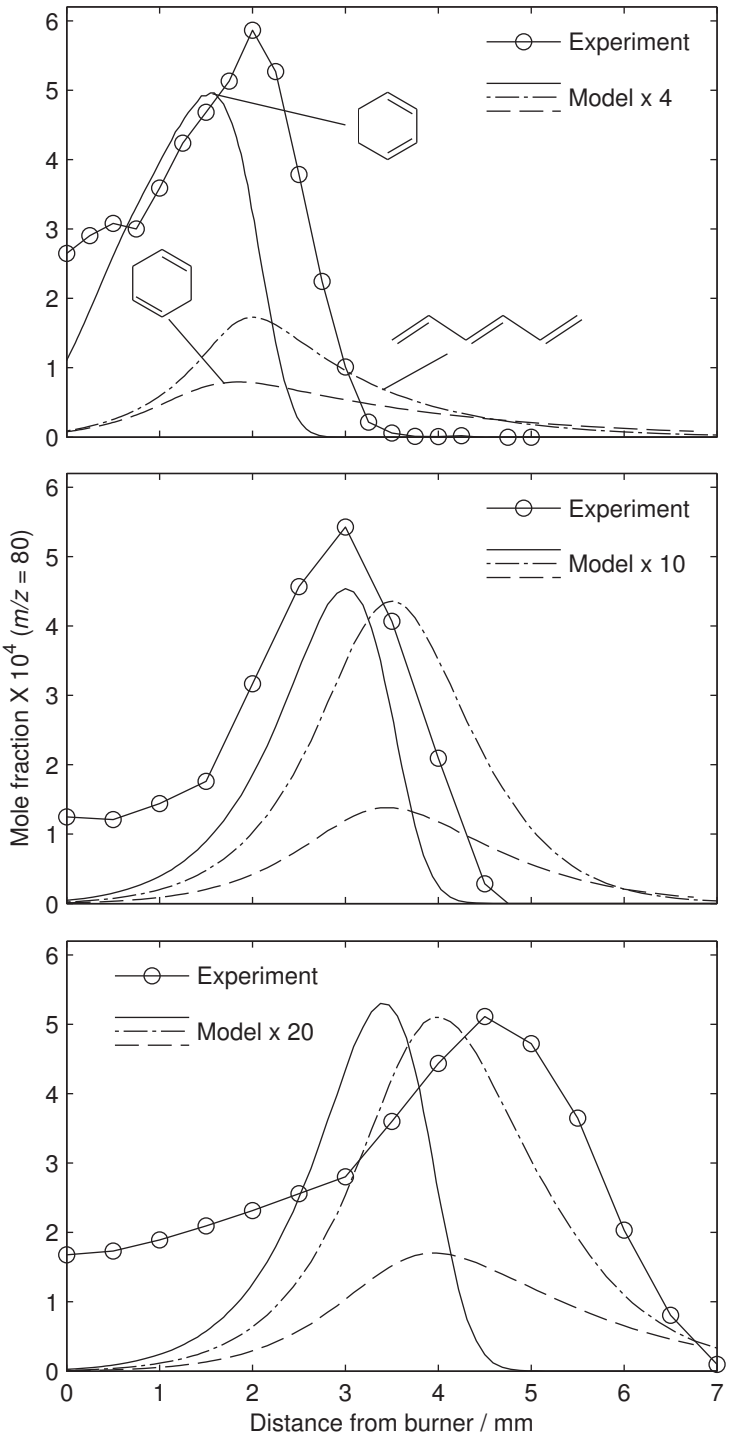
Experiment
Model x 4
Experiment
Model x 10
Experiment
Model x 20
Mole fraction X 10^4 (m/z = 80)
Distance from burner / mm
0
1
2
3
4
5
6
7

Figure 15

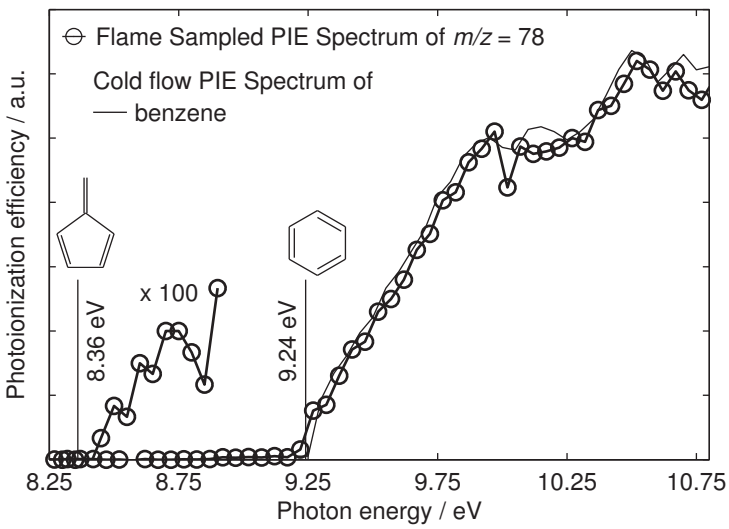
Flame Sampled PIE Spectrum of m/z = 78
Cold flow PIE Spectrum of
benzene
x 100
8.36 eV
9.24 eV
Photoionization efficiency / a.u.
8.25
8.75
9.25
9.75
10.25
10.75
Photon energy / eV

Figure 16

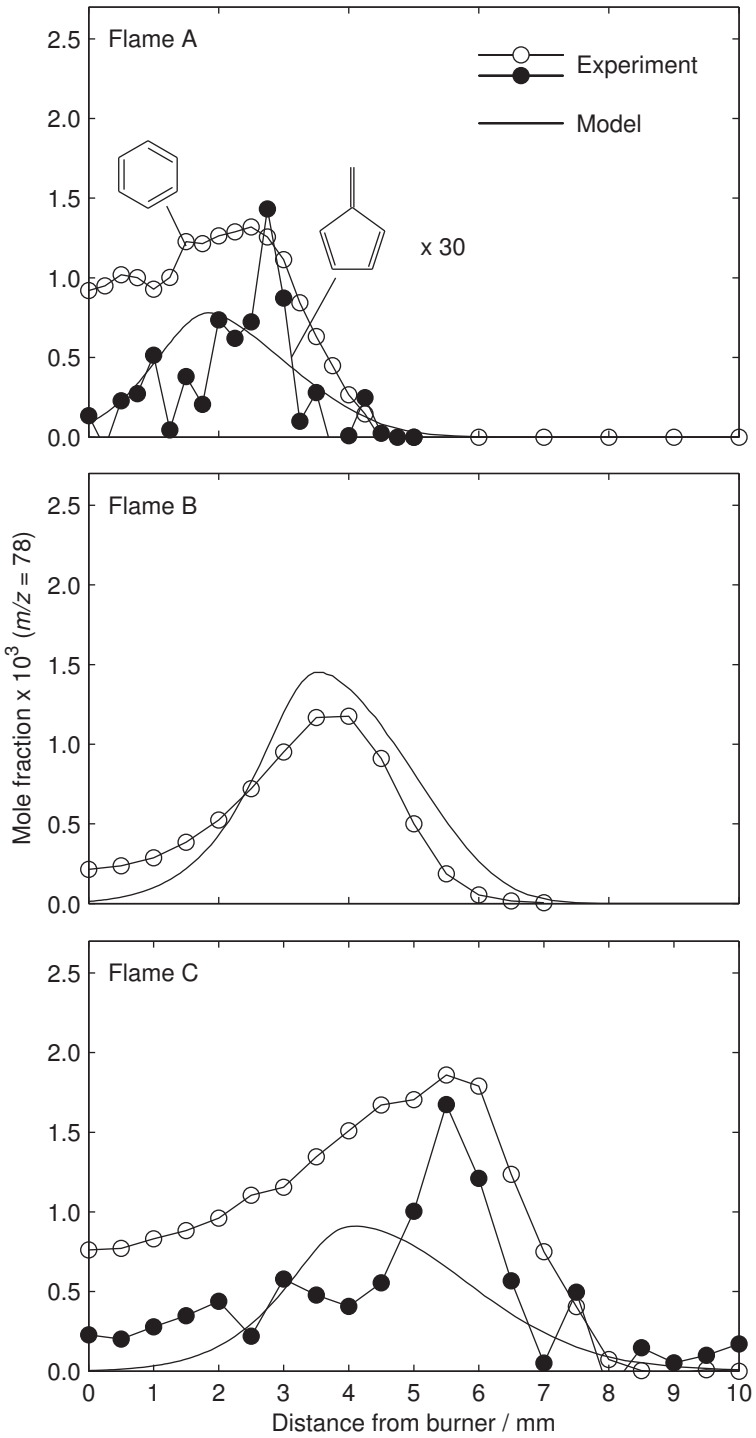
Flame A
Experiment
Model
x 30
Flame B
Flame C
Mole fraction x 10^3 (m/z = 78)
Distance from burner / mm
0.0
0.5
1.0
1.5
2.0
2.5
0
1
2
3
4
5
6
7
8
9
10

Figure 17